

Modelling and predicting soil carbon sequestration: is current model structure fit for purpose?

Mohammad Javad Davoudabadi^{*1,2,3,4}, Daniel Pagendam⁴, Christopher Drovandi^{1,2,3}, Jeff Baldock⁵, and Gentry White^{1,2,3}

¹*School of Mathematical Sciences, Queensland University of Technology, Australia;*

²*Australian Research Council Centre of Excellence for Mathematical & Statistical Frontiers (ACEMS);*

³*QUT Centre for Data Science, Queensland University of Technology, Australia;*

⁴*CSIRO Data61, GPO Box 2583, Brisbane, QLD 4001, Australia;*

⁵*CSIRO Agriculture & Food, Glen Osmond, South Australia, Australia;*

Abstract

Soil carbon accounting and prediction play a key role in building decision support systems for land managers selling carbon credits, in the spirit of the Paris and Kyoto protocol agreements. Land managers typically rely on computationally complex models fit using sparse datasets to make these accountings and predictions. The model complexity and sparsity of the data can lead to over-fitting, leading to inaccurate results using new data or making predictions. Modellers address over-fitting by simplifying their models, neglecting some soil organic carbon (SOC) components. In this study, we introduce two novel SOC models and a new RothC-like model and investigate how the SOC components and complexity of the SOC models affect the SOC prediction in the presence of small and sparse time series data. We develop model selection methods that can identify the soil carbon model with the best predictive performance, in light of the available data. Through this analysis we reveal that commonly used complex soil carbon models can over-fit in the presence of sparse time series data, and our simpler models can produce more accurate predictions.

*mohammadjavad.davoudabadi@hdr.qut.edu.au

Keywords: Soil carbon sequestration; State-space model ; Rao-Blackwellised particle filter; Correlated pseudo-marginal method; Leave-future-out cross-validation; Model selection.

1 Introduction

Large-scale carbon emission from soil (one of the planet’s major carbon reservoirs) into the atmosphere has deleterious impacts on global climate change, soil quality, and crop productivity (Adams et al., 2011; Shi et al., 2020). Soil organic carbon (SOC) could be used as a significant global sink for atmospheric carbon through land-management practices, helping to reduce the atmospheric concentration of greenhouse gases and improving agricultural productivity.

International bodies and agreements such as the Intergovernmental Panel on Climate Change (IPCC) and the Paris and Kyoto Protocol agreements mitigate global warming by assessing the science related to climate change and reduce greenhouse gas emissions, especially CO_2 . These agreements adopted systems of carbon accounting and trading markets. A part of these carbon markets (tracking and trading) is related to selling carbon credits by farmers and land-holders who apply land-management practices to sequester carbon and track the change of soil carbon sequestration in their farmlands. They usually have small datasets for tracking the changes in soil carbon as SOC sampling is time-consuming and costly.

Markets can quantify changes in soil carbon stocks using accurate models of soil carbon turnover and sequestration. Such models can also help develop a deeper understanding of the sequestration process and forecast future changes and trends in SOC. Researchers have developed computer-simulation models such as RothC (Jenkinson et al., 1987), and Century (Parton et al., 1988) to help make inferences about trends in carbon stocks using time series of measurements collected over many years. For example, to improve the accounting of field emissions in the carbon footprint of agricultural products, Peter et al. (2016) assess the change of SOC based on simulations with the RothC model in one of the IPCC methodological approaches (Tier 3) and compare it with other default IPCC methods. At their core, models such as RothC partition the total SOC mass into specific pools. These pools are decomposable plant material (DPM), resistant plant matter (RPM), humified organic matter (HUM), microbial biomass (BIO), and inert organic matter (IOM) (Adams et al., 2011; Capon et al., 2010).

Research using statistical models, sensitivity analysis (running models for different sets of parameter values), or simulated climate change attempts to quantify uncertainties in soil carbon

turnover (Jones et al., 2007; Koo et al., 2007; Post et al., 2008; Juston et al., 2010; Paul et al., 2003; Stamati et al., 2013). Clifford et al. (2014) quantified uncertainties in model inputs, dynamics, and uncertainties in model parameters for a one pool soil carbon in a comprehensive manner using a physical-statistical model for carbon dynamics within a framework known as Bayesian hierarchical modelling (BHM). The statistical methods used by Clifford et al. (2014) can be computationally burdensome, especially for more complex models such as some models we consider in this study. In addition, differences between the various soil carbon pools (DPM, RPM, HUM, BIO and IOM) are ignored in Clifford et al. (2014). More recent studies consider the interactions of microbes in a microbially-based SOC model (SOMic version 1.0) (Woolf and Lehmann, 2019). Other studies compare the fit of linear and non-linear soil biogeochemical models (SBMs) using data assimilation with soil respiration data sourced from a meta-analysis of soil warming studies (Xie et al., 2020).

In this study, we explore the effect of relaxing some of the bio-geochemical realism of models such as RothC with respect to predicting soil carbon stocks. Our focus is using these models with the temporally sparse datasets typically available for assessing trends in soil carbon on farms, making use of two datasets from Tarlee in South Australia and Brigalow in Queensland, Australia (Clifford et al., 2014; Skjemstad et al., 2004). These two sites are in different climatic regions, and it shows we can apply our approaches to any dataset of any climatic region. A pertinent scientific question is whether multi-pool models such as RothC are too complex relative to the limited data that is often available to fit them. Therefore, we understand how model predictive performance varies when we amalgamate some of these conceptual pools in the underlying process dynamics. Specifically, we consider: (i) a single pool model considering soil carbon as a homogeneous pool that can decay and release carbon into the atmosphere (Clifford et al., 2014); (ii) a two-pool model in which we consider a single homogeneous pool of decomposable SOC and an IOM pool that does not decompose; (iii) a three-pool model which considers two pools of decomposable SOC (one of them represents the biological pool) and the IOM pool; and (iv) a five-pool model considering all pools mentioned above present in RothC. The two and three-pool models are novel soil carbon models that we introduce in this study. Also, the five-pool model is a novel soil carbon model in terms of the modelling framework and its simplification in terms of time step and parameters as our datasets are not large enough to estimate some parameters in the RothC model.

Our modelling framework predicts changes in soil carbon stocks and accounts for epistemic uncertainty (uncertainty in the bio-geochemical process dynamics) in a statistically defensible manner. This is particularly important in the present context. We explore structural differences

in the systems of equations used to describe soil carbon process dynamics which is one of the major differences between our statistical approach and that used in the simpler regression studies (e.g. Xie et al., 2020; Sokol and Bradford, 2019). We develop a state-space modelling framework (used for a one-pool model by (Davoudabadi et al., 2020; Clifford et al., 2014)) to the two, three, and RothC-like five-pool models. We develop a Bayesian model selection method (leave-future-out cross-validation (LFO-CV) (Bürkner et al., 2020)) to choose, for a given dataset, the best soil carbon model in terms of its out-of-sample predictive accuracy. Our approach optimally adapts to the data at hand. In this study, we show the three-pool model outperforms the five-pool model despite its bio-geochemical realism. This demonstrates that modellers and soil scientists should consider the volume and quality of data available for making inferences when defining the level of detail and realism included in statistical soil carbon models. We avoid fitting overly complex soil models in the presence of sparse data and it is important when making predictions about soil carbon stocks; otherwise a land-owner might unwittingly enter into a contract to sequester carbon that has a higher risk than anticipated. Conversely, when data are sufficiently informative, our approach supports more complexity. In addition, we explore the effect of microbes and inert organic matter on the carbon cycle decomposition by adding biomass and IOM pools in the one-pool model, and show that by adding these pools, we obtain better soil carbon prediction than the one-pool model in Clifford et al. (2014).

We organise the rest of the paper as follows. In Section 2 the structure of the models is described. In Section 3, we compare the models based on their out-of-sample predictive accuracy. We quantify the uncertainty of our estimate in Section 4. Section 5 presents a discussion of this study and our results. We introduce our model framework and the LFO-CV criterion in Section 6.

2 Model Structure

The total SOC consists of different components defined by their origin and their decay rate. These components originate from living organisms known as biotic material or non-living (abiotic) material (Adams et al., 2011; Lal, 2010). Based on the RothC model, the components of the total SOC include DPM, RPM, HUM, BIO, IOM (Adams et al., 2011; Capon et al., 2010). The one-pool model in Clifford et al. (2014) considered all components mentioned above as a single pool. The process model of the one-pool model is a combination of linear and non-linear sub-models. The details of the process and the observation models of these sub-models are shown in the supple-

mentary material Sections E.1 and E.2, respectively. Figure 1a graphically represents the carbon emission process in the one-pool model. Based on Figure 1a, a fraction of carbon decays is emitted into the atmosphere as CO_2 and the rest remains in the pool.

In the two-pool model, we consider the IOM pool as a second pool that is resistant to chemical and biological reactions and encompasses charcoal or charred material (Capon et al., 2010). The IOM fraction is not subject to biological transformation and is thus constant (Falloon et al., 2000). As the IOM fraction is constant, its process model at time t is a constant value and should be estimated. The process and the observation models of the two-pool model are presented respectively in Sections F.1 and F.2. Figure 1b shows the graphical representation of the two-pool model.

The three-pool model considers the IOM and BIO as separate pools with a main pool of decomposable carbon (an amalgamation of DPM, RPM, and HUM pools). Soil carbon decomposes from the decomposable carbon pool, and fractions are either transferred to the BIO pool or lost to the atmosphere as CO_2 . Carbon present in the BIO pool that decomposes is either lost to the atmosphere as CO_2 , re-assimilated as biological mass or transferred to the main soil carbon pool. Figure 1c shows the diagram of the carbon emission in the three-pool model. The process and observation models of the three-pool model are presented in detail in Sections G.1 and G.2 of the supplementary material, respectively. It is noteworthy to mention that the size of the microbial pool encompasses a small fraction of the total organic carbon (e.g. 5% of the TOC). We implement this constraint by rejecting BIO state trajectories that exceed 5% of the TOC in the Markov chain Monte Carlo (MCMC) algorithm.

The RothC model, consisting of five conceptual pools, is the standard soil carbon used in many studies and is considered a reasonable representation of the physical sub-species of carbon in the soil. In the models presented so far, we have considered the pools to be either one of the RothC pools or an amalgamation of the five RothC pools. In the five-pool model presented here, we now retain the structure presented in the RothC model without any amalgamation.

In the five-pool model, plant material is split between two conceptual pools: DPM and RPM. Decomposition of carbon from these two pools either leaves the system as CO_2 or is transformed to carbon in the BIO and HUM pools. Carbon from the BIO and HUM pools that decomposes can either be lost to the atmosphere as CO_2 , or transformed to carbon in the BIO or HUM pools. The process and observation models of the carbon transfer in the five-pool model are presented mathematically in detail in Section H of the supplementary material. The five-pool model is depicted in Figure 1d.

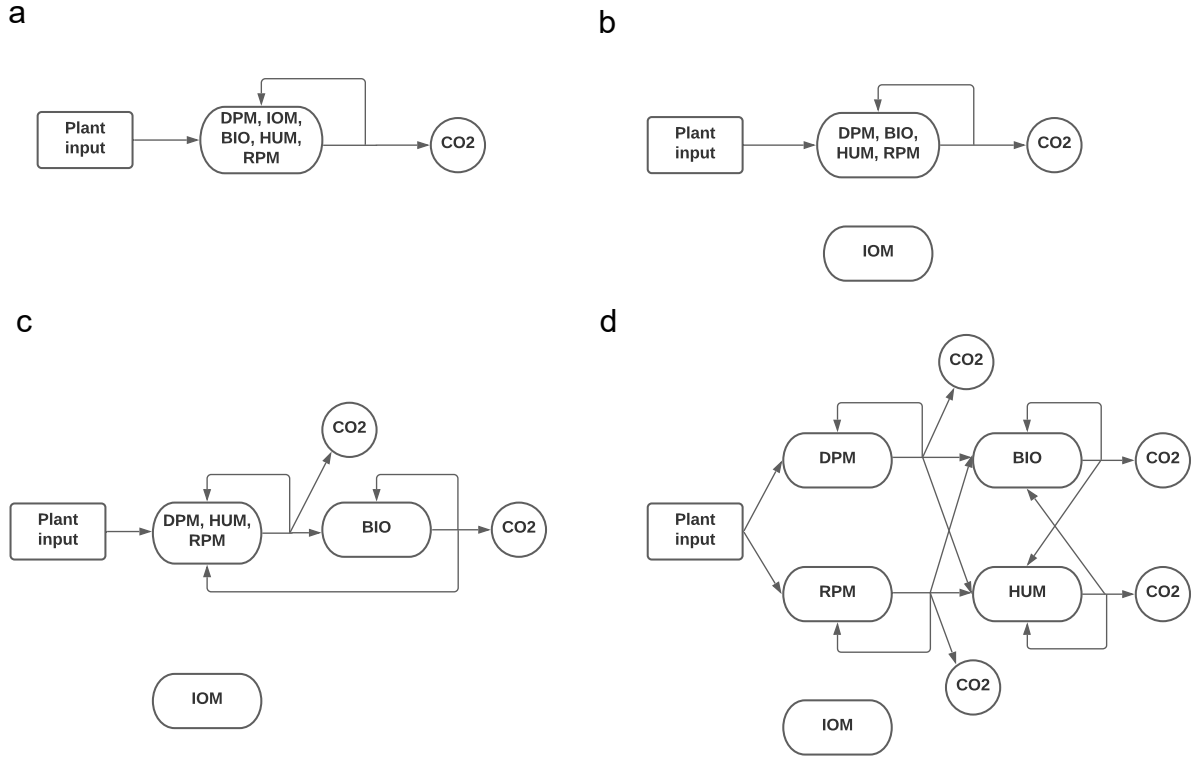


Figure 1: Graphical representation of the carbon emission in the a) one-pool model, b) two-pool model, c) three-pool model, and d) five-pool model. The five pools from RothC have been amalgamated into a single homogeneous soil carbon pool in the one-pool model. The DPM, BIO, HUM and RPM pools are amalgamated and treated as a single homogeneous pool in the two-pool model, and the DPM, HUM and RPM pools are amalgamated and treated as a single homogeneous pool in the three-pool model.

3 Comparing Models

We worked with four MCMC chains, each initialised with a randomly sampled parameter vector, in the Correlated Pseudo-marginal Method (CPM) method for estimating the predictive density (4). We ran each chain for 200,000 iterations discarding the first 80,000 as burn-in. We thinned these chains, choosing every 30th sample of the MCMC samples to estimate (4), therefore, S in equation (4) was equal to 4,000. The minimum numbers of observations, L , used for making predictions for future data in the Tarlee and Brigalow datasets were 12 and 13, respectively. The estimated expected log pointwise predictive density (ELPD) of the one, two, three, and five-pool models applied on the Tarlee dataset were -53.02 , -40.55 , -34.79 , and -37 , respectively. The estimated ELPD of those models applied on the Brigalow dataset were -36.89 , -36.88 , -36.48 , and -49.57 , respectively. Based on these results (supplementary material Tables 15 and 16), the three-pool

model outperformed the other models in the sense of yielding the best LFO predictive ability for both the Brigalow and Tarlee datasets. This three-pool model included an inert carbon pool and two decomposable pools that were conceptually equivalent to a biological pool (the decomposers) and a decomposable material pool, an amalgamation of DPM, RPM, and HUM pools. For Tarlee, the five-pool RothC-like model had the next best ELPD, but in Brigalow, the five-pool model exhibited the worst ELPD of the four models studied. The performances of the three and five-pool models in estimating the trajectories of the SOC dynamics of the Brigalow dataset are highlighted visually in Figure 2a and 2b, respectively. As shown in Figure 2b, the five-pool model increased uncertainty in the soil carbon dynamics, especially during the sparse periods, typified by wide 95% credible intervals.

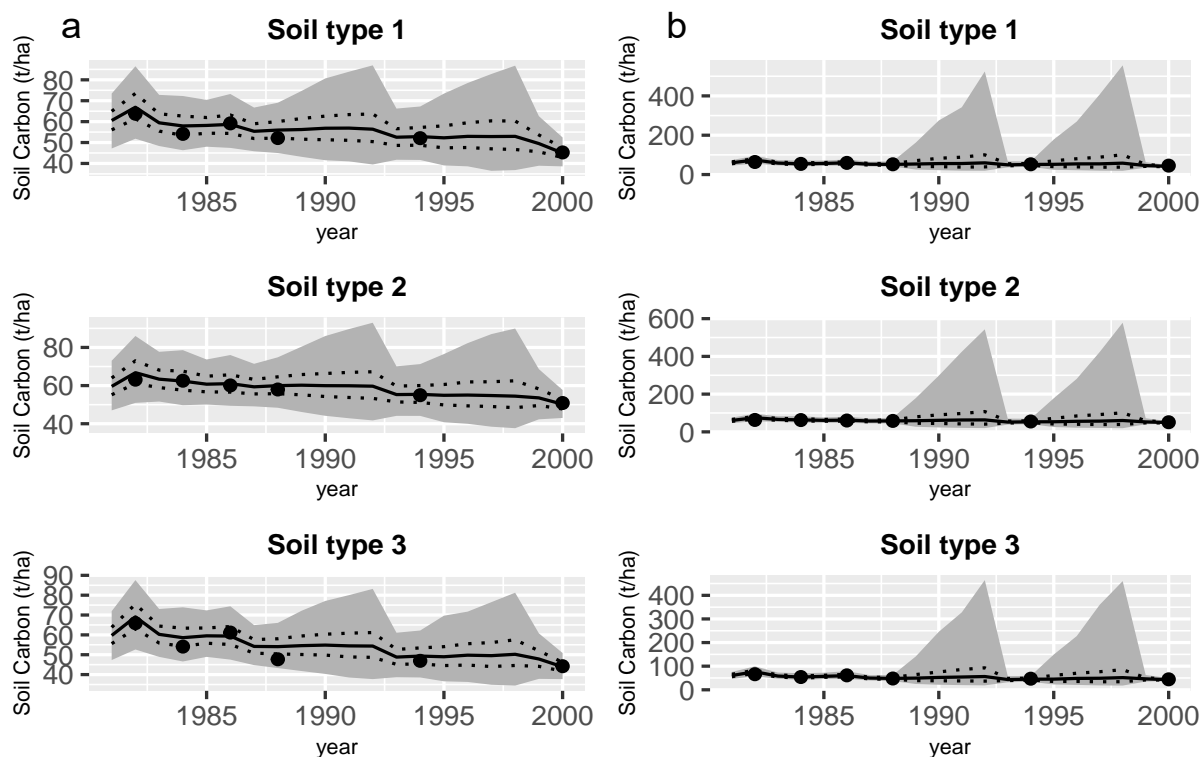


Figure 2: Soil organic carbon (SOC) dynamics of the Brigalow dataset based on a) the three-pool model and b) the five-pool model. The gray shaded part is the area between the 2.5th and the 97.5th percentiles for the SOC process gained by the three and five-pool models. The 25th and the 75th percentiles for the SOC process are indicated by the dashed lines. The 50th percentile is shown by the solid line and the measured SOC values are indicated by filled dots.

Setting aside the five-pool model and focussing on the one, two, and three-pool models, we see that amongst these three models, the ranking from best to worst is three-pool, two-pool, and one-pool for both study sites. Although the three-pool model has the largest ELPD, we cannot say with full confidence it is the best model compared to the one and two-pool models as there is not much difference between their estimated ELPDs acknowledging the Monte Carlo errors. Reducing the

Monte Carlo error to identify the preferred model more precisely would require running the MCMC chains for many more iterations, which would be very computationally intensive. Ultimately, there does not appear to be a strong preference between one to three pool models for the Brigalow dataset.

4 Uncertainty quantification

We can quantify the uncertainty of our estimate in many ways, for example, through a 95% credible interval or the estimated expected value of functionals of interest. The inference about the mass of SOC added over a period of time can be achieved through the MCMC samples of the posterior distribution. We represent the posterior distribution $p(\mathbf{X}, \boldsymbol{\theta} | \mathbf{Y})$ by M^* samples $\{(X^m, \boldsymbol{\theta}^m) : m = 1, \dots, M^*\}$ and the posterior expectation of any function $g^*(\mathbf{X}, \boldsymbol{\theta})$ can be estimated by these samples. Here θ , Y , and X are the unknown parameters, observations, unobserved state process, respectively.

$$\mathbf{E}(g^*(\mathbf{X}, \boldsymbol{\theta}) | \mathbf{Y}) \approx \frac{1}{M^*} \sum_{m=1}^{M^*} g^*(X^m, \boldsymbol{\theta}^m).$$

The error of the accuracy of such estimates is negligible for sufficiently large sample size M^* . In the CPM method, we worked with 4 chains each initialised with a randomly sampled parameter vector. We ran each chain for 200,000 iterations with the first 80,000 discarded as burn-in.

The change in SOC to field i between 1978 and following year t in the Tarlee dataset is considered as follows

$$g^*(\mathbf{X}, \boldsymbol{\theta}) = X_{TOC(t)}^i - X_{TOC(1978)}^i;$$

and can be estimated as follows

$$\hat{g}^*(\mathbf{X}, \boldsymbol{\theta}) = \mathbf{E}(X_{TOC(t)}^i - X_{TOC(1978)}^i | \mathbf{Y});$$

where $X_{TOC(t)}^i$ in the three-pool model is equal to the summation of $X_{C(t)}^i$, $X_{IOM(t)}^i$, and $X_{B(t)}^i$. The posterior variance, $\text{var}(X_{TOC(t)}^i - X_{TOC(1978)}^i | \mathbf{Y})$, is a measure of uncertainty associated with this Bayes estimate. The average of the SOC change between 1978 and 1997 in fields 1, 2, and 3 in the Tarlee trial based on the three-pool model were -3.81 , -3.47 , and 7.12 , respectively (Figure 3a). Here the negative values denote that the first two fields were expected to lose carbon over

the 20-year period. The management strategies that are used in fields 1, 2, and 3 are “Wheat-Wheat”, “Wheat-Fallow”, and “Wheat-Pasture”, respectively. This average for three soil types of the Brigalow dataset, based on the three-pool model, between 1981 and 2000 were -4.37 , -0.43 , and -5.13 , respectively (Figure 3b).

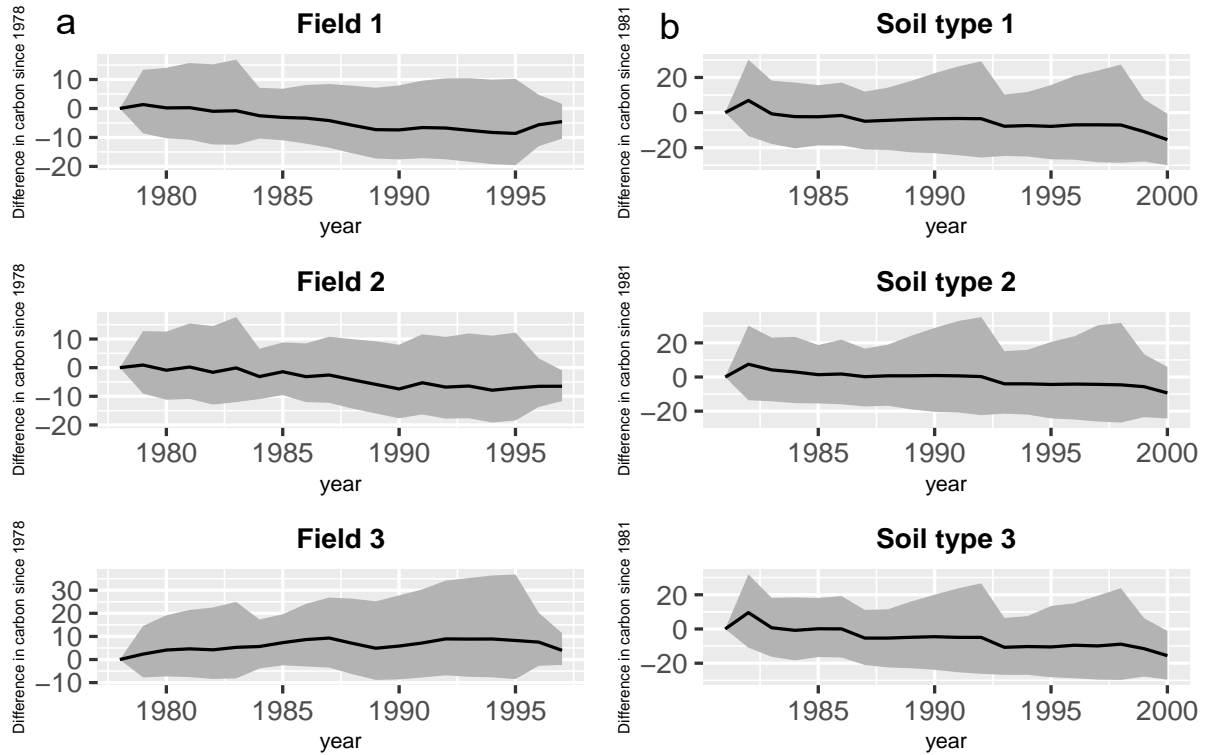


Figure 3: The expected difference of the SOC in each year from 1978 and 1981 in the a) Tarlee and b) Brigalow datasets, respectively, estimated based on the three-pool model. The change of the SOC stock in each field/soil type is indicated by solid line, and the gray shaded part is the area between the 2.5th and the 97.5th percentiles for the SOC process.

We can find the 95% credible interval for the amount of carbon in the soil and lost to the soil by computing the upper and lower limits of the interval which are the 97.5th and 2.5th percentiles of the posterior distribution, respectively. These percentiles for the SOC process of each soil type in the Brigalow trial and each Tarlee field are presented in Figures 2a and 4, respectively. We also show the 95% credible interval and 50th percentile for the carbon emitted from the soil as carbon dioxide for both Tarlee and Brigalow sites in Figure 5a and 5b, respectively.

We calculated the Gelman and Rubin’s convergence diagnostics, \hat{R} for the model parameters of the three-pool model of the Tarlee dataset and the one-pool model of the Brigalow dataset. They are presented in Tables 13 and 14, respectively, in Section I of the supplementary material.

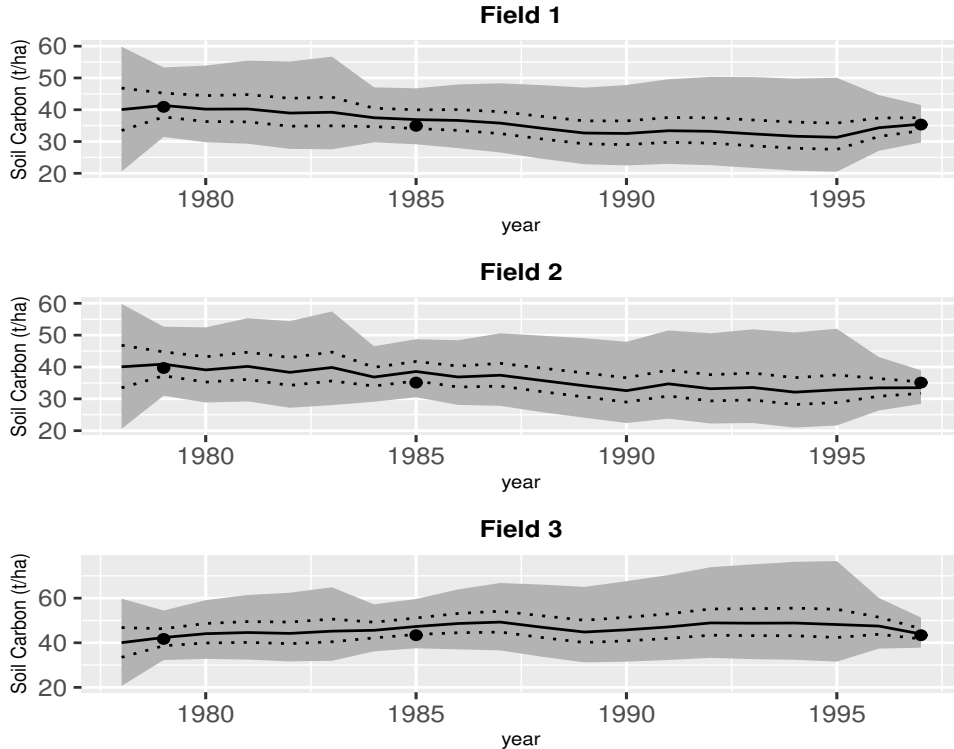


Figure 4: Soil organic carbon (SOC) dynamics in the three Tarlee fields. The gray shaded part is the area between the 2.5th and the 97.5th percentiles for the SOC process gained by the three-pool model. The 25th and the 75th percentiles for the SOC process are indicated by the dashed lines. The 50th percentile is shown by the solid line and the measured SOC values are indicated by filled dots.

5 Discussion

In this study, we have developed three new soil carbon models and compared them with the one-pool model in Clifford et al. (2014) in the BHM framework, which allows us to think conditionally and critically about the parameters, the process, and the data that reside within a soil carbon model. To show these models are broadly applicable, we have implemented them on two datasets.

An important motivating question behind this study is whether multi-pool models such as RothC are fit for making inferences on soil carbon dynamics in (commonly occurring) situations where soil carbon measurements are monitored infrequently. In fitting models to two Australian datasets, we found a three-pool model (in both the cases of Tarlee and Brigalow) to have the best predictive ability of those models considered and to be better than a five-pool model, which is frequently adopted for its bio-geochemical realism. We conclude that the detail and realism included in statistical soil carbon models should consider the volume and quality of data available for making inferences. Indeed, this study has shown that some concessions in physical realism can lead to better predictive accuracy. This can be helpful for the IPCC, Paris agreement and Kyoto protocol's purposes, especially for national carbon accounting where datasets are sparse.

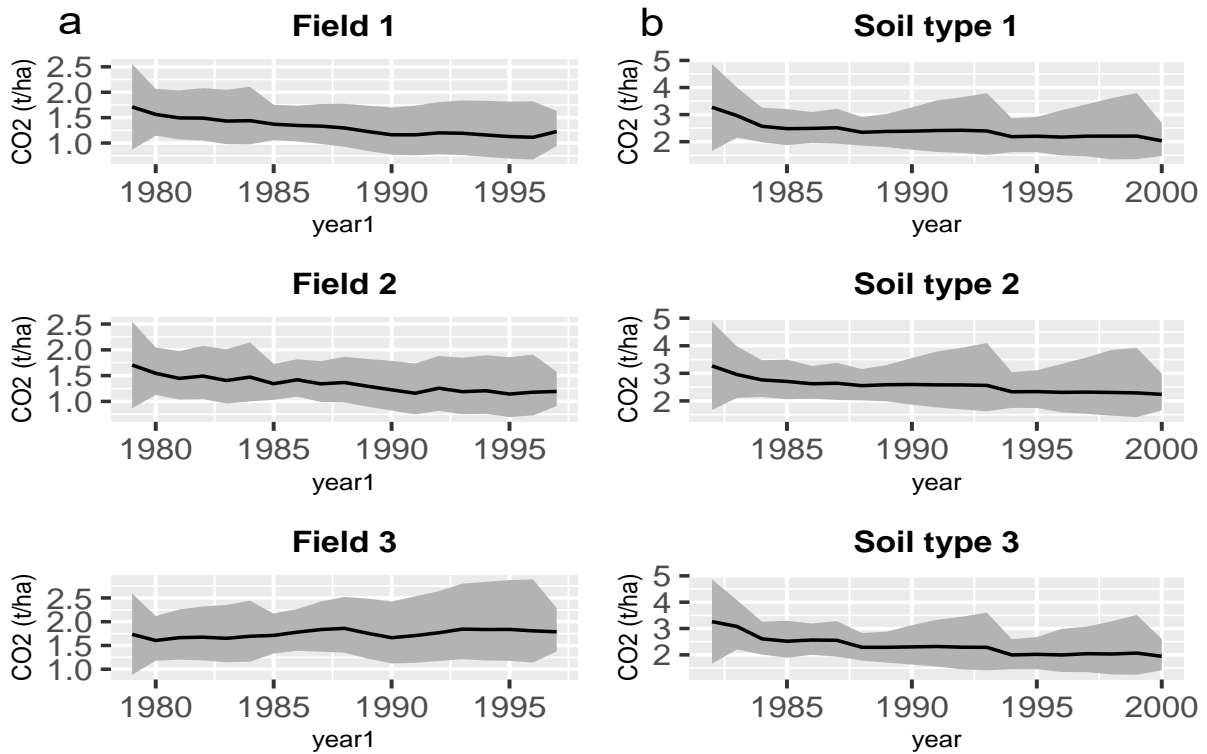


Figure 5: The amount of carbon emitted from a) each field of the Tarlee site b) each soil type of the Brigalow site into the atmosphere, estimated based on the three-pool model. The gray shaded region is the area between the 25th and the 97.5th percentiles and the solid line represents the 50th percentile.

Furthermore, we have explored the effect of microbes and inert organic matter on the carbon cycle decomposition by adding biomass and IOM pools in the Tarlee model in (Clifford et al., 2014). In particular, based on the LFO-CV criterion, we have shown that the three-pool model, which includes biomass and IOM pools, outperforms other models on the Tarlee and Brigalow datasets. The LFO-CV of the five-pool model is close to the three-pool model in its predictive ability for Tarlee but not for Brigalow. Both the Brigalow and Tarlee datasets exhibit relatively long, multi-year periods with no observation of any carbon pools (i.e. temporally sparse data). During those periods, all knowledge about the soil carbon process comes from the carbon inputs, the process dynamics and the model parameters. However, in the case of Brigalow, adding more pools to the model increased uncertainty in the soil carbon dynamics in each iteration of the particle filter process, causing poor predictive performance, typified by wide 95% credible interval during those sparse periods. This result indicated that multi-pool models might not be as fit-for-purpose (compared to some simpler models) when used with sparse data over time.

In exploring soil carbon models with reduced complexity, we chose not to investigate a four-pool model. We could create such a model by combining the DPM and RPM components, for example. However, we deemed a four pool model to be too similar in structure to the five pool model,

therefore not providing much additional variation in model complexity. Furthermore, our aims in this study were to explore the importance of microbe and inert organic matter pools because they are fundamentally different from other soil carbon pools (the former being constrained in its total pool size and the latter being stable over very long time scales). The range of models used in this study provides valuable insight into whether the complexity of the RothC model is warranted when datasets are temporally sparse.

We have shown that, the three-pool model that was found to be best suited to the Brigalow and Tarlee datasets in this study can be used to obtain good fits to observational data and can be used to estimate (with uncertainty) the net gain or loss of carbon (overtime) at each study site.

Since both datasets used in this study are not large, we have used the LFO-CV criterion for model evaluation. It is noteworthy to mention that this criterion is computationally expensive when used with a larger dataset since it requires repeating the MCMC every time a data point is introduced. Based on our experiences here, other criteria such as Pareto smoothed importance sampling LFO-CV (PSIS-LFO-CV) (Bürkner et al., 2020) or widely applicable information criterion (WAIC) (Watanabe and Opper, 2010) may be more relevant methods for large datasets.

We have successfully demonstrated applying advanced Bayesian methods in Davoudabadi et al. (2020) to a range of more complex soil carbon models. We have shown that these methods can be used for inference on soil carbon dynamics and advocate these methods where a rigorous quantification of uncertainty is important.

In this study, we consider the effect of the biomass pool on the carbon emission decomposition rate with the limitation on the maximum size of microbes, which is 5% of the total SOC. Through this limitation, we have prevented too much carbon from entering the microbial pool and where excess, we have ignored that extra amount of carbon in the microbial pool. We could improve the growth of the population of microbes by considering a dynamic process in future studies. We can fit a model (e.g. perhaps a logistic population model with a carrying capacity) to the growth of the size of microbes. In this case, the extra amount of carbon in the BIO pool can be diverted into the other pools into which carbon can be cycled. We will consider this in future research.

6 Methods

6.1 Soil Carbon Model

Modelling soil carbon sequestration would help land-holders understand the risks of putting their sequestered carbon into a trading scheme. Governments forecast changes in soil carbon stocks as part of national carbon accounts. To this end, we identify and quantify sources of uncertainty in soil carbon sequestration, and we address them within a Bayesian hierarchical modelling framework.

We can consider uncertainties in a dynamical SOC model as arising from three sources: errors in the observations, randomness or uncertainty inherent in the underlying physical processes, and uncertainties in model parameters (Clifford et al., 2014). These uncertainties are modelled through the observation model $p(\mathbf{Y}|\mathbf{X}, \boldsymbol{\theta})$, the process model $p(\mathbf{X}|\boldsymbol{\theta})$, and the prior $p(\boldsymbol{\theta})$ where $p(\cdot)$, and $p(\cdot|E)$ denote the probability density function of the enclosed random variable, and the conditional probability density function given the event E , respectively. These three models form a hierarchical framework known as a Bayesian Hierarchical Model (BHM). The top-level of the hierarchy contains the observation model followed by the process model, located at the second level, and the third level underneath these two levels contains the parameter model (Allenby and Rossi, 2006; Berliner, 1996; Cressie and Wikle, 2015). A BHM is represented mathematically as follows:

$$p(\mathbf{Y}, \mathbf{X}, \boldsymbol{\theta}) = p(\mathbf{Y}, \mathbf{X}|\boldsymbol{\theta})p(\boldsymbol{\theta}) = p(\mathbf{Y}|\mathbf{X}, \boldsymbol{\theta})p(\mathbf{X}|\boldsymbol{\theta})p(\boldsymbol{\theta}). \quad (1)$$

Note that the joint distribution $p(\mathbf{Y}, \mathbf{X}, \boldsymbol{\theta})$ captures all the uncertainty in the model. The advantage of analysing a model within the BHM framework is that it incorporates prior knowledge related to the parameters into the analysis by updating the distributions of these parameters with observed data. The latent physical state of the SOC, \mathbf{X} , evolves as a dynamical process and given noisy, sparse data. Inferences about soil carbon dynamics, parameters, and functions of them can be made through the posterior distribution $p(\mathbf{X}, \boldsymbol{\theta}|\mathbf{Y})$. We can write the posterior distribution based on (1) as follows:

$$p(\mathbf{X}, \boldsymbol{\theta}|\mathbf{Y}) = \frac{p(\mathbf{Y}|\mathbf{X}, \boldsymbol{\theta})p(\mathbf{X}|\boldsymbol{\theta})p(\boldsymbol{\theta})}{p(\mathbf{Y})} \quad (2)$$

where $p(\mathbf{Y})$ depends only on data and may be difficult to calculate analytically or numerically, thus the posterior itself may be difficult to evaluate. Fortunately, one can draw samples from the

posterior if it is not analytically tractable.

As in other recent statistical analyses (Davoudabadi et al., 2020; Clifford et al., 2014) we use a state-space modelling framework (the first and second levels of the BHM) to predict changes in soil carbon stocks. State-space models are more challenging to fit in practice than simpler regression models (used in (Xie et al., 2020; Sokol and Bradford, 2019)) because they acknowledge uncertainty in the latent process dynamics. The prior information of the parameter model (the third level of the BHM) is described in the following.

6.2 Prior Information

As mentioned earlier, the process model and the observation model typically depend on unknown parameters, and the parameter model captures the uncertainty around these parameters. A Bayesian approach for model fitting is applied to quantify the uncertainty in parameters and predictions. This approach places a prior distribution on the unknown parameter vector $\boldsymbol{\theta}$, which is the advantage of using the Bayesian analysis since we implement our prior knowledge of parameters as part of the inferential process.

In general, the prior knowledge about parameters includes three categories: informative, weakly informative, and uninformative priors. When we have a small dataset or the dataset is sparse, the prior distribution becomes more influential and informative priors can become more useful. In this study, we obtain priors from previous studies (Clifford et al., 2014; Davoudabadi et al., 2020; Skjemstad et al., 2004) and expert opinion. The model parameters and their prior probability density functions are listed in Tables 4 and 5 (Section C) of the supplementary material.

6.3 Posterior Distribution Inference

To estimate the changes in SOC over time as a result of the various management practices, and to estimate the parameters driving the sequestration of carbon, we sample from the posterior distribution $p(X_{TOC}, \boldsymbol{\theta} | \mathbf{Y})$, where X_{TOC} is the mass of total SOC. To this end, we draw samples from the posterior distribution $p(\mathbf{X}, \boldsymbol{\theta} | \mathbf{Y})$ in (2) which can be decomposed into two components $p(\mathbf{X} | \boldsymbol{\theta}, \mathbf{Y})p(\boldsymbol{\theta} | \mathbf{Y})$ and we preserve the components related to the SOC process X_{TOC} and its parameters $\boldsymbol{\theta}$. Davoudabadi et al. (2020) used advanced Bayesian methods (e.g. correlated pseudo-marginal (CPM) method and the Rao-Blackwellised particle filters (RBPF) for state-space models) to reduce the computational cost of estimating uncertainties in the one-pool model presented by

(Clifford et al., 2014). The CPM method, one of several particle Markov chain Monte Carlo (PMCMC) methods, is applied to the model to draw samples from $p(\boldsymbol{\theta}|\mathbf{Y})$ as the resulting likelihood is not tractable (Deligiannidis et al., 2018; Davoudabadi et al., 2020). The CPM method in Davoudabadi et al. (2020) outperforms other state of the art PMCMC methods in terms of computation time. The advantage of using this method is that it reduces the computational cost of estimating intractable likelihoods by correlating the estimators of the likelihoods in the acceptance ratio of its algorithm (Section D.3 of the supplementary material provides the CPM algorithm, 3). This correlation can be achieved by correlating the auxiliary random numbers used to obtain these estimators; see Deligiannidis et al. (2018); Davoudabadi et al. (2020) for more details. To estimate the marginal likelihood of the state variables, we use the RBPF as the SOC model combines linear and non-linear sub-models. The RBPF algorithm estimates the marginal likelihood of the non-linear sub-model through bootstrap particle filter (BPF). It computes the marginal likelihood of the linear part of the model through the Kalman Filter (KF) algorithm (Doucet et al., 2000; Davoudabadi et al., 2020). Computing the exact likelihood of the linear sub-model makes the RBPF algorithm an attractive algorithm in these scenarios as it reduces the computational cost of the estimated likelihood dramatically. See (Davoudabadi et al., 2020) for more details about the RBPF, BPF and KF algorithms. In addition, the algorithm of the KF and BPF methods are provided in Sections D.1 and D.2, Algorithms 1 and 2, respectively. The RBPF algorithm is reused to draw a sample of the state process from the posterior distribution $p(X_{TOC}|\boldsymbol{\theta}, \mathbf{Y})$. In the CPM algorithm, it is required to generate candidate parameters from appropriate proposal distributions. The proposal distributions are presented in the supplementary material Section C.

We assess the quality of the MCMC samples through an MCMC diagnostic known as the Gelman and Rubin’s convergence diagnostic statistic (Gelman and Rubin, 1992). The Gelman and Rubin’s convergence diagnostic statistic, \hat{R} , can be used to assess whether the MCMC samples have “mixed” sufficiently (effectively sampling from the probability distribution) and have reached a stationary distribution (Gelman and Rubin, 1992). Gelman and Rubin’s convergence diagnostic compares samples from multiple chains to assess whether the output from each chain is sufficiently similar to the others. The output from each chain is indistinguishable when the scale reduction factor estimated from the sampling is less than 1.2.

Before estimating model parameters and conducting inference with a model, it is essential to validate our model to establish its suitability for estimating changes in soil carbon stocks. In the next section, we introduce our method for selecting between competing soil carbon models,

focusing on predictive accuracy.

6.4 Model Evaluation

One way to evaluate a model or compare different models is to measure predictive accuracy (Gelman et al., 2014). As our models depend on time, for model comparison and selection, we apply leave-future-out cross-validation (LFO-CV) that refits a model to different subsets of the data (Bürkner et al., 2020). The LFO-CV is a fully Bayesian metric in that it uses the entire posterior distribution. This method is the approach used to compare the model’s predictive accuracy for the four SOC models listed in Section 2. We would like to explore the predictive accuracy of simpler models of soil carbon dynamics through model comparison to understand whether more complex multi-pool models offer the best predictive tool when the datasets available for inference are relatively sparse.

Let $Y_{1:T}$ be a time series of observations and let L be the minimum number of observations from the series that we will require before making predictions for future data. We can learn enough about the time series to predict future observations (Bürkner et al., 2020). We would like to compute the predictive densities $p(\tilde{Y}_{t+1}|Y_{1:t})$ for each $t \in \{L, \dots, T-1\}$ where \tilde{Y}_{t+1} is a future vector of observed data. The expected log pointwise predictive density (ELPD) can be used as a global measure of predictive accuracy, which is

$$\text{ELPD} = \log \prod_{t=L}^{T-1} \mathbf{E}_{\theta|Y_{1:t}}(p(\tilde{Y}_{t+1}|Y_{1:t}, \theta)) = \sum_{t=L}^{T-1} \log \int p(\tilde{Y}_{t+1}|Y_{1:t}, \theta)p(\theta|Y_{1:t}) d\theta. \quad (3)$$

In practice, the integral in (3) is intractable, however we can approximate it through Monte-Carlo methods (Bürkner et al., 2020). To estimate $p(\tilde{Y}_{t+1}|Y_{1:t})$, we draw samples $(\theta_{1:t}^1, \dots, \theta_{1:t}^S)$ from the posterior distribution $p(\theta|Y_{1:t})$ for $t \in \{1, \dots, \gamma\}$ where $\gamma \in \{L, \dots, T-1\}$ using the particle MCMC method described in Section 6.3 and estimate the predictive density for $\tilde{Y}_{L+1:T}$ as follows

$$p(\tilde{Y}_{t+1}|Y_{1:t}) \approx \frac{1}{S} \sum_{s=1}^S p(\tilde{Y}_{t+1}|Y_{1:t}, \theta_{1:t}^s). \quad (4)$$

When our model is a state-space model, we need to consider the state variables as part of the parameter space and estimate them through the particle filter methods to apply the LFO-CV. The reason for selecting ELPD instead of other global measures of accuracy such as the root mean squared error (RMSE) is that it evaluates a distribution to provide a measure of out-of-sample predictive performance rather than evaluating a point estimate (like the mean or median), which

we see as favourable from a Bayesian perspective (Vehtari et al., 2012; Bürkner et al., 2020).

Acknowledgments

We would like to thank CSIRO for providing the data used in this study. MJD was supported by QUT-CSIRO Digital Agriculture Scholarship and a CSIRO Digital Agriculture Top-Up Scholarship. CD was supported by an Australian Research Council Discovery Project (DP200102101). We gratefully acknowledge the computational resources provided by QUT's High Performance Computing (HPC) and Research Support Group.

References

- Adams, M., Crawford, J., Field, D., Henakaarchchi, N., Jenkins, M., McBratney, A., de Remy de Courcelles, V., Singh, K., Stockmann, U., and Wheeler, J. (2011). Managing the soil-plant system to mitigate atmospheric CO₂. Technical report, Discussion paper for the Soil Carbon Sequestration Summit, 31 January-2 February 2011. The United States Studies Centre at the University of Sydney.
- Allenby, G. M. and Rossi, P. E. (2006). Hierarchical Bayes models. *The Handbook of Marketing Research: Uses, Misuses, and Future Advances*, pages 418–440.
- Berliner, L. M. (1996). Hierarchical Bayesian time series models. In *Maximum entropy and Bayesian methods*, pages 15–22. Springer.
- Bürkner, P.-C., Gabry, J., and Vehtari, A. (2020). Approximate leave-future-out cross-validation for Bayesian time series models. *Journal of Statistical Computation and Simulation*, pages 1–25.
- Capon, T., Harris, M., and Reeson, A. (2010). Soil carbon sequestration market based instruments (mbis): A literature review. *University of Sydney, Sydney*.
- Clifford, D., Pagendam, D., Baldock, J., Cressie, N., Farquharson, R., Farrell, M., Macdonald, L., and Murray, L. (2014). Rethinking soil carbon modelling: a stochastic approach to quantify uncertainties. *Environmetrics*, 25(4):265–278.
- Cressie, N. and Wikle, C. K. (2015). *Statistics for Spatio-Temporal Data*. John Wiley & Sons.
- Davoudabadi, M. J., Pagendam, D., Drovandi, C., Baldock, J., and White, G. (2020). Advanced Bayesian approaches for state-space models with a case study on soil carbon sequestration. *Environmental Modelling & Software*, page 104919.
- Deligiannidis, G., Doucet, A., and Pitt, M. K. (2018). The correlated pseudomarginal method. *Journal of the Royal Statistical Society: Series B (Statistical Methodology)*, 80(5):839–870.
- Doucet, A., De Freitas, N., Murphy, K., and Russell, S. (2000). Rao-Blackwellised particle filtering for dynamic Bayesian networks. In *Proceedings of the Sixteenth conference on Uncertainty in Artificial Intelligence*, pages 176–183. Morgan Kaufmann Publishers Inc.

- Falloon, P., Smith, P., Coleman, K., and Marshall, S. (2000). How important is inert organic matter for predictive soil carbon modelling using the Rothamsted carbon model? *Soil Biology and Biochemistry*, 32(3):433–436.
- Gelman, A., Hwang, J., and Vehtari, A. (2014). Understanding predictive information criteria for Bayesian models. *Statistics and computing*, 24(6):997–1016.
- Gelman, A. and Rubin, D. B. (1992). Inference from iterative simulation using multiple sequences. *Statistical Science*, 7(4):457–472.
- Jenkinson, D. S., Hart, P. B. S., Rayner, J. H., and Parry, L. C. (1987). Modelling the turnover of organic matter in long-term experiments at Rothamsted. *INTECOL Bulletin*, 15:1–8.
- Jones, J. W., Koo, J., Naab, J. B., Bostick, W. M., Traore, S., and Graham, W. D. (2007). Integrating stochastic models and in situ sampling for monitoring soil carbon sequestration. *Agricultural Systems*, 94(1):52–62.
- Juston, J., Andrén, O., Kätterer, T., and Jansson, P. (2010). Uncertainty analyses for calibrating a soil carbon balance model to agricultural field trial data in Sweden and Kenya. *Ecological Modelling*, 221(16):1880–1888.
- Koo, J., Bostick, W. M., Naab, J. B., Jones, J. W., Graham, W. D., and Gijsman, A. J. (2007). Estimating soil carbon in agricultural systems using ensemble Kalman filter and DSSAT-Century. *Transactions of the ASABE*, 50(5):1851–1865.
- Lal, R. (2010). Managing soils and ecosystems for mitigating anthropogenic carbon emissions and advancing global food security. *BioScience*, 60(9):708–721.
- Luo, Z., Wang, E., and Sun, O. J. (2010). Soil carbon change and its responses to agricultural practices in Australian agro-ecosystems: a review and synthesis. *Geoderma*, 155(3):211–223.
- Parton, W. J., Stewart, J. W., and Cole, C. V. (1988). Dynamics of C, N, P and S in grassland soils: a model. *Biogeochemistry*, 5(1):109–131.
- Paul, K. I., Polglase, P. J., and Richards, G. P. (2003). Sensitivity analysis of predicted change in soil carbon following afforestation. *Ecological Modelling*, 164(2-3):137–152.

- Peter, C., Fiore, A., Hagemann, U., Nendel, C., and Xiloyannis, C. (2016). Improving the accounting of field emissions in the carbon footprint of agricultural products: a comparison of default ipcc methods with readily available medium-effort modeling approaches. *The International Journal of Life Cycle Assessment*, 21(6):791–805.
- Post, J., Hattermann, F. F., Krysanova, V., and Suckow, F. (2008). Parameter and input data uncertainty estimation for the assessment of long-term soil organic carbon dynamics. *Environmental Modelling & Software*, 23(2):125–138.
- Shi, Z., Allison, S. D., He, Y., Levine, P. A., Hoyt, A. M., Beem-Miller, J., Zhu, Q., Wieder, W. R., Trumbore, S., and Randerson, J. T. (2020). The age distribution of global soil carbon inferred from radiocarbon measurements. *Nature Geoscience*, 13(8):555–559.
- Skjemstad, J. O., Spouncer, L. R., Cowie, B., and Swift, R. S. (2004). Calibration of the Rothamsted organic carbon turnover model (RothC ver. 26.3), using measurable soil organic carbon pools. *Soil Research*, 42(1):79–88.
- Skjemstad, t. J. and Spouncer, L. (2003). NCAS calibration and verification data. v1. *CSIRO. Data Collection*.
- Sokol, N. W. and Bradford, M. A. (2019). Microbial formation of stable soil carbon is more efficient from belowground than aboveground input. *Nature Geoscience*, 12(1):46–53.
- Stamati, F. E., Nikolaidis, N. P., and Schnoor, J. L. (2013). Modeling topsoil carbon sequestration in two contrasting crop production to set-aside conversions with RothC—calibration issues and uncertainty analysis. *Agriculture, Ecosystems & Environment*, 165:190–200.
- Vehtari, A., Ojanen, J., et al. (2012). A survey of Bayesian predictive methods for model assessment, selection and comparison. *Statistics Surveys*, 6:142–228.
- Watanabe, S. and Opper, M. (2010). Asymptotic equivalence of Bayes cross validation and widely applicable information criterion in singular learning theory. *Journal of Machine Learning research*, 11(12).
- Woolf, D. and Lehmann, J. (2019). Microbial models with minimal mineral protection can explain long-term soil organic carbon persistence. *Scientific reports*, 9(1):1–8.

Xie, H. W., Romero-Olivares, A. L., Guindani, M., and Allison, S. D. (2020). A Bayesian approach to evaluation of soil biogeochemical models. *Biogeosciences*, 17(15):4043–4057.

Supplementary Material

A Background and Description of Datasets

Our model selection method is motivated by two datasets that are collected from two locations in Australia. The details of these sites are presented in the following.

A.1 Tarlee Dataset

An agricultural research experiment site known as Tarlee situated 80 km north of Adelaide, South Australia was established in 1977 to examine the impact of management practices on agricultural productivity as a long term field experiment (Skjemstad and Spouncer, 2003). The soil of this site is classified as a hard-setting red-brown earth with sandy loam texture. This site has a Mediterranean climate and is dominated by winter rainfall with an average of 355 mm from April to October (Clifford et al., 2014; Luo et al., 2010; Skjemstad et al., 2004). Soil properties of that site were monitored over a 20-year period in three fields under different management practices. Table 1 presents the time period of management treatments that were implemented in three trial fields in Tarlee.

Management treatments	Field 1	Field 2	Field 3
Wheat for grain	(1979 - 1987) and (1990 - 1996)	-	-
Wheat for hay	1988 and 1989	1989	-
Fallow	1997	1997	1997
Wheat for grain and fallow	-	(1979 - 1988) and (1990 - 1996)	-
Wheat and pasture	-	-	(1979 - 1987)
Wheat and pasture for hay	-	-	1988 and 1989
Wheat for grain and pasture	-	-	(1990 - 1996)

Table 1: The duration of management treatments in three fields in Tarlee.

A.2 Brigalow Dataset

Brigalow is a research station in Queensland, Australia. This site is situated in a semi-arid, and subtropical climate, and consists of three forested catchments of 12-17 ha (Skjemstad et al., 2004). Three monitoring sites were established within each of the catchments in recognition of three soil types (a duplex soil and two clays). One catchment was planted to wheat and occasional sorghum and the other to buffel pasture and the last one was left under native Brigalow forest. At this site, on one catchment, after clearing land under Brigalow (*Acacia harpophylla*) in 1982, continuous wheat with some sorghum was established over a 18-year period. Table 2 shows the duration of management practices in Brigalow.

Management treatments	Soil type 1	Soil type 2	Soil type 3
Cleared	1982	1982	1982
Wheat for grain	(1985 - 1992) and (1994, 1996, 1998)	(1985 - 1992) (1994, 1996, 1998)	(1985 - 1992) (1994, 1996, 1998)
Sorghum for grain	1984, 1995, 1997 and 1999	1984, 1995, 1997 and 1999	1984, 1995, 1997 and 1999
Fallow	1983 and 1993	1983 and 1993	1983 and 1993

Table 2: The duration of management treatments in Brigalow.

In the next section, we present the notations used in this study.

B Notation

The notations related to latent variables \mathbf{X} at time t and field i , their corresponding measured values \mathbf{Y} and some model parameters are presented in Table 3.

All processes and all observations at time t in all fields (soil types) are denoted by $X_{(t)} = (X_{(t)}^1, X_{(t)}^2, X_{(t)}^3)$ and $Y_{(t)} = (Y_{(t)}^1, Y_{(t)}^2, Y_{(t)}^3)$, respectively. All processes at all fields (soil types) and all times are represented by \mathbf{X} , and \mathbf{Y} represents all available data. We denote a set of variables as $Y_{1:t} = (Y_{(1)}, \dots, Y_{(t)})$. The log-normal distribution is denoted by $LN(\mu_1, \sigma_1^2)$ with mean parameter μ_1 and variance parameter σ_1^2 for a log transformation of the random variable. $N(\mu_2, \sigma_2^2)$ represents the normal distribution with mean and variance μ_2 and σ_2^2 , respectively. Some other notations are presented wherever they are required.

Notation	Description
$X_{C(t)}^i$	The mass of SOC (t/ha)
$X_{W(t)}^i$	The mass of total wheat dry matter (t/ha)
$X_{S(t)}^i$	The mass of total sorghum dry matter (t/ha)
$X_{G_W(t)}^i$	The mass of total grain dry matter produced from wheat (t/ha)
$X_{G_S(t)}^i$	The mass of total grain dry matter produced from sorghum (t/ha)
$X_{P(t)}^i$	The mass of total pasture dry matter (t/ha)
$X_{IOM(t)}^i$	The mass of IOM (t/ha)
$X_{B(t)}^i$	The mass of BIO (t/ha)
$X_{D(t)}^i$	The mass of DPM (t/ha)
$X_{R(t)}^i$	The mass of resistant plant material (RPM) (t/ha)
$X_{H(t)}^i$	The mass of HUM (t/ha)
$Y_{TOC(t)}^i$	The measured value of total SOC (t/ha)
$Y_{W(t)}^i$	The measured value of total wheat dry matter (t/ha)
$Y_{S(t)}^i$	The measured value of total sorghum dry matter (t/ha)
$Y_{G_W(t)}^i$	The measured value of total wheat grain dry matter (t/ha)
$Y_{G_S(t)}^i$	The measured value of total sorghum grain dry matter (t/ha)
$Y_{P(t)}^i$	The measured value of total pasture dry matter (t/ha)
$Y_{IOM(t)}^i$	The measured value of IOM (t/ha)
$Y_{H(t)}^i$	The measured value of HUM (t/ha)
$Y_{POC(t)}^i$	The measured value of POC (t/ha)
K_C	The decay rate of total SOC (Y^{-1})
K_A	The decay rate of the carbon in pool A (Y^{-1})
π_{AB}	Proportion of the mass of carbon transfer from carbon pool A to carbon pool B
Δt	The yearly time step
P_D	Proportion of the carbon input that added to the DPM pool

Table 3: The notations of latent variables, their corresponding measured values and some model parameters.

C Prior and Proposal Distributions

The model parameters and their prior probability density functions related to the Tarlee and Brigalow datasets are listed in Tables 4 and 5 (to avoid repetition, the priors of the model parameters which have the same distribution in both datasets are presented in Table 4).

The proposal density functions of the one, two, and three-pool models applied on the Tarlee dataset are presented in Table 6. In the three-pool model, the proposal density functions of some parameters are different from the ones in the one and two-pool models, therefore, we show them in Table 7. The proposal density functions of the five-pool model related to the Tarlee dataset are shown in Table 8. Tables 9, 10, 11, and 12 show respectively the proposal density functions of the one, two, three, and five-pool models related to the Brigalow dataset. To avoid repetition, the

Parameter	Prior	Type
$X_{C(1978)}^1$	Truncated-normal($40, 10^2, lower = 0$)	Uninformative
$X_{C(1978)}^2$	Truncated-normal($40, 10^2, lower = 0$)	Uninformative
$X_{C(1978)}^3$	Truncated-normal($40, 10^2, lower = 0$)	Uninformative
X_{IOM}	Truncated-normal($4, 0.5^2, lower = 0$)	Uninformative
K_C	LN($-2.71, (0.127)^2$)	Informative
K_D	LN($-2.71, (0.127)^2$)	Informative
K_B	Truncated-normal($0.66, 0.3^2, lower = 0$)	Informative
K_R	LN($-2.5, (0.135)^2$)	Informative
K_H	Truncated-normal($0.02, 0.01^2, lower = 0$)	Informative
c	N($0.45, (0.01)^2$)	Informative
r_W	N($0.5, (0.067)^2$)	Informative
r_P	N($1, (0.125)^2$)	Informative
p	Beta($89.9, 809.1$)	Informative
h_W	LN($0.825, (0.36)^2$)	Weakly Informative
μ_{G_W}	N($0.42, (1.18)^2$)	Weakly Informative
μ_P	N($1.41, (1.81)^2$)	Weakly Informative
ρ_{G_W}	Uniform($-1, 1$)	Uninformative
ρ_P	Uniform($-1, 1$)	Uninformative
σ_η^2	Inv-gamma($0.001, 0.001$)	Uninformative
$\sigma_{\eta_C}^2$	Inv-gamma($0.001, 0.001$)	Uninformative
$\sigma_{\eta_D}^2$	Inv-gamma($0.001, 0.001$)	Uninformative
$\sigma_{\eta_B}^2$	Inv-gamma($0.001, 0.001$)	Uninformative
$\sigma_{\eta_R}^2$	Inv-gamma($0.01, 0.01$)	Uninformative
$\sigma_{\eta_H}^2$	Inv-gamma($0.001, 0.001$)	Uninformative
$\sigma_{G_W}^2$	Inv-gamma($0.001, 0.001$)	Uninformative
σ_W^2	Inv-gamma($0.001, 0.001$)	Uninformative
σ_P^2	Inv-gamma($0.001, 0.001$)	Uninformative
π_{DH}	Uniform($0, 1$)	Uninformative
π_{RH}	Uniform($0, 1$)	Uninformative
π_{HH}	Uniform($0, 1$)	Uninformative
π_{BH}	Uniform($0, 1$)	Uninformative
π_{DB}	Uniform($0, 1$)	Uninformative
π_{RB}	Uniform($0, 1$)	Uninformative
π_{HB}	Uniform($0, 1$)	Uninformative
π_{BB}	Uniform($0, 1$)	Uninformative
π_{CB}	Uniform($0, 1$)	Uninformative
π_{BC}	Uniform($0, 1$)	Uninformative
$\sigma_{\epsilon_{TOC}}^2$	0.025	Fixed
$\sigma_{\epsilon_{POC}}^2$	0.9	Fixed
$\sigma_{\epsilon_{G_W}}^2$	0.023	Fixed
$\sigma_{\epsilon_W}^2$	0.133	Fixed
$\sigma_{\epsilon_P}^2$	0.067	Fixed
$\sigma_{\epsilon_{IOM}}^2$	0.01	Fixed
$\sigma_{\epsilon_H}^2$	0.1	Fixed

Table 4: Prior distributions of parameters of the Tarlee dataset and the ones are common in both datasets.

Parameter	Prior	Type
$X_{C(1981)}^1$	Truncated-normal($60, 15^2, lower = 0$)	Uninformative
$X_{C(1981)}^2$	Truncated-normal($60, 15^2, lower = 0$)	Uninformative
$X_{C(1981)}^3$	Truncated-normal($60, 15^2, lower = 0$)	Uninformative
X_{IOM}	Truncated-normal($12, 2^2, lower = 0$)	Uninformative
h_S	LN($0.46, (1.6)^2$)	Informative
ρ_{G_S}	Uniform($-1, 1$)	Uninformative
μ_{G_S}	N($0.42, (1.18)^2$)	Weakly Informative
r_S	N($0.5, (0.067)^2$)	Informative
K_R	Truncated-normal($0.15, 0.075^2, lower = 0$)	Informative
$\sigma_{G_S}^2$	Inv-gamma($0.001, 0.001$)	Uninformative
$\sigma_{\eta_B}^2$	Truncated-normal($0, 0.5^2, lower = 0$)	Weakly Informative
$\sigma_{\eta_R}^2$	Truncated-normal($0, 0.5^2, lower = 0$)	Weakly Informative
$\sigma_{\eta_H}^2$	Truncated-normal($0, 0.5^2, lower = 0$)	Weakly Informative
σ_S^2	Inv-gamma($0.001, 0.001$)	Uninformative
$\sigma_{\epsilon_{G_S}}^2$	0.023	Fixed
$\sigma_{\epsilon_S}^2$	0.133	Fixed

Table 5: Prior distributions of parameters of the Brigalow dataset.

proposal density functions of parameters which are the same in two or three-pool model are not shown in Tables 11 and 12.

D State-space Model

The state-space model uses observable measurement variable $Y_{(t)}$ and unobserved state variable $X_{(t)}$ which can be estimated through observational data that depend on the state variable, to describe a system. This model includes the first two levels of the hierarchy of the BHM framework and its generic representation with Gaussian noise is

$$\begin{aligned}
X_{(t)} &= f(X_{(t-1)}) + \mathbf{B}u_{(t)} + \epsilon_{(t)} \\
Y_{(t)} &= g(X_{(t)}) + \nu_{(t)};
\end{aligned} \tag{5}$$

where $\epsilon_{(t)} \sim N(\mu, \sigma_X^2)$ and $\nu_{(t)} \sim N(\lambda, \sigma_Y^2)$ are state and measurement noise components, respectively and the control-input matrix \mathbf{B} is applied to a known vector of inputs $u_{(t)}$. The aim is to produce estimators for the state variable $X_{(t)}$ through the filtering distribution $p(X_{(t)}|Y_{1:t})$. When the filtering distribution does not have a closed-form expression some methods such as the Kalman filter (KF) (in the case of linear-Gaussian model) and particle filter can be used to approximate it. For the sake of simplicity, we assume the static parameter θ is fixed in this section.

Parameter	Proposal
K_C	$N(K_C, 0.001^2)$
K_B	Truncated-normal($K_B, 0.09^2, lower = 0$)
c	Truncated-normal($c, 0.005^2, lower = 0, upper = 1$)
r_W	Truncated-normal($r_W, 0.05^2, lower = 0$)
r_P	Truncated-normal($r_P, 0.05^2, lower = 0$)
p	Truncated-normal($p, 0.005^2, lower = 0, upper = 1$)
h_W	Truncated-normal($h_W, 0.05^2, lower = 0$)
μ_{G_W}	$N(\mu_{G_W}, 0.05^2)$
μ_P	$N(\mu_P, 0.05^2)$
ρ_{G_W}	Truncated-normal($\rho_{G_W}, 0.05^2, lower = -1, upper = 1$)
ρ_P	Truncated-normal($\rho_P, 0.1^2, lower = -1, upper = 1$)
σ_η^2	Truncated-normal($\sigma_\eta^2, 0.001^2, lower = 0$)
$\sigma_{\eta_C}^2$	Truncated-normal($\sigma_{\eta_C}^2, 0.001^2, lower = 0$)
$\sigma_{\eta_B}^2$	Truncated-normal($\sigma_{\eta_B}^2, 0.01^2, lower = 0$)
$\sigma_{G_W}^2$	Truncated-normal($\sigma_{G_W}^2, \frac{\sigma_{G_W}^2}{20^2}, lower = 0$)
σ_W^2	Truncated-normal($\sigma_W^2, 0.001^2, lower = 0$)
σ_P^2	Truncated-normal($\sigma_P^2, 0.1^2, lower = 0$)
π_{CB}	Truncated-normal($\pi_{CB}, 0.05^2, lower = 0, upper = 1$)
π_{BC}	Truncated-normal($\pi_{BC}, 0.1^2, lower = 0, upper = 1$)
π_{BB}	Truncated-normal($\pi_{BB}, 0.1^2, lower = 0, upper = 1$)
$X_{C(1978)}^1$	Truncated-normal($X_{C(1978)}^1, 5^2, lower = 0$)
$X_{C(1978)}^2$	Truncated-normal($X_{C(1978)}^2, 5^2, lower = 0$)
$X_{C(1978)}^3$	Truncated-normal($X_{C(1978)}^3, 5^2, lower = 0$)
X_{IOM}	Truncated-normal($X_{IOM}, 0.9^2, lower = 0$)

Table 6: Proposal distributions of one, two, and three-pool models used in the CPM method for the Tarlee dataset.

Parameter	Proposal
K_C	$N(K_C, 0.005^2)$
μ_G	$N(\mu_G, 0.075^2)$
μ_P	$N(\mu_P, 0.1^2)$
$X_{C(1978)}^1$	Truncated-normal($X_{C(1978)}^1, 2^2, lower = 0$)
$X_{C(1978)}^2$	Truncated-normal($X_{C(1978)}^2, 2^2, lower = 0$)
$X_{C(1978)}^3$	Truncated-normal($X_{C(1978)}^3, 2^2, lower = 0$)
X_{IOM}	Truncated-normal($X_{IOM}, 0.09^2, lower = 0$)

Table 7: Proposal distributions of some parameters in the three-pool model used in the CPM method for the Tarlee dataset.

D.1 Kalman Filter

In the case of linear-Gaussian state-space model, the KF can be used to estimate state variable as an efficient method since it is an optimal estimator in the sense of minimising the variance of the

Parameter	Proposal
K_D	Truncated-normal($K_D, 0.005^2, lower = 0$)
K_B	Truncated-normal($K_B, 0.09^2, lower = 0$)
K_R	Truncated-normal($K_R, 0.005^2, lower = 0$)
K_H	Truncated-normal($K_H, 0.006^2, lower = 0$)
c	Truncated-normal($c, 0.005^2, lower = 0, upper = 1$)
r_W	Truncated-normal($r_W, 0.05^2, lower = 0$)
r_P	Truncated-normal($r_P, 0.05^2, lower = 0$)
p	Truncated-normal($p, 0.005^2, lower = 0, upper = 1$)
h	Truncated-normal($h, 0.05^2, lower = 0$)
μ_G	$N(K, 0.075^2)$
μ_P	$N(K, 0.1^2)$
ρ_G	Truncated-normal($\rho_G, 0.25^2, lower = -1, upper = 1$)
ρ_P	Truncated-normal($\rho_P, 0.2^2, lower = -1, upper = 1$)
$\sigma_{\eta D}^2$	Truncated-normal($\sigma_{\eta D}^2, 0.1^2, lower = 0$)
σ_G^2	Truncated-normal($\sigma_G^2, \frac{\sigma_G^2}{20^2}, lower = 0$)
σ_W^2	Truncated-normal($\sigma_W^2, 0.01^2, lower = 0$)
σ_P^2	Truncated-normal($\sigma_P^2, 0.1^2, lower = 0$)
X_{IOM}	Truncated-normal($X_{IOM}, 0.09^2, lower = 0$)
$X_{C(1978)}^1$	Truncated-normal($X_{C(1978)}^1, 1.3^2, lower = 0$)
$X_{C(1978)}^2$	Truncated-normal($X_{C(1978)}^2, 1.3^2, lower = 0$)
$X_{C(1978)}^3$	Truncated-normal($X_{C(1978)}^3, 1.3^2, lower = 0$)
$\sigma_{\eta B}^2$	Truncated-normal($\sigma_{\eta B}^2, 0.1^2, lower = 0$)
P_D	Truncated-normal($P_D, 0.15^2, lower = 0, upper = 1$)
σ_R^2	Truncated-normal($\sigma_R^2, 0.09^2, lower = 0$)
σ_H^2	Truncated-normal($\sigma_H^2, 0.01^2, lower = 0$)
π_{DB}	Truncated-normal($\pi_{DB}, 0.05^2, lower = 0, upper = 1$)
π_{BB}	Truncated-normal($\pi_{BB}, 0.15^2, lower = 0, upper = 1$)
π_{DH}	Truncated-normal($\pi_{DH}, 0.09^2, lower = 0, upper = 1$)
π_{RH}	Truncated-normal($\pi_{RH}, 0.1^2, lower = 0, upper = 1$)
π_{HH}	Truncated-normal($\pi_{HH}, 0.1^2, lower = 0, upper = 1$)
π_{BH}	Truncated-normal($\pi_{BH}, 0.015^2, lower = 0, upper = 1$)
π_{RB}	Truncated-normal($\pi_{RB}, 0.09^2, lower = 0, upper = 1$)
π_{HB}	Truncated-normal($\pi_{HB}, 0.1^2, lower = 0, upper = 1$)

Table 8: Proposal distributions of the five-pool model used in the CPM method for the Tarlee dataset.

estimated state. The linear-Gaussian state-space model has the form

$$X_{(t)} = \mathbf{A}^* X_{(t-1)} + \mathbf{B}^* u_{(t)} + \epsilon_{(t)}^*$$

$$Y_{(t)} = \mathbf{C}^* X_{(t)} + \nu_{(t)}^*;$$

where $\epsilon_{(t)}^* \sim N(\mathbf{0}, \mathbf{Q}^*)$, $\nu_{(t)}^* \sim N(\mathbf{0}, \mathbf{R}^*)$, \mathbf{A}^* is the state-transition matrix, the control-input matrix \mathbf{B}^* is applied to a known vector of inputs $u_{(t)}$, and \mathbf{C}^* is the observation matrix. The KF method is shown in Algorithm 1, here $MVN(\boldsymbol{\mu}, \boldsymbol{\Sigma})$ denotes the multivariate normal density with mean vector

Parameter	Proposal
K_C	$N(K_C, 0.002^2)$
c	Truncated-normal($c, 0.005^2, lower = 0, upper = 1$)
r_W	Truncated-normal($r_W, 0.05^2, lower = 0$)
p	Truncated-normal($p, 0.005^2, lower = 0, upper = 1$)
h_W	Truncated-normal($h_W, 0.05^2, lower = 0$)
μ_{G_W}	$N(\mu_{G_W}, 0.05^2)$
ρ_{G_W}	Truncated-normal($\rho_{G_W}, 0.05^2, lower = -1, upper = 1$)
σ_η^2	Truncated-normal($\sigma_\eta^2, 0.001^2, lower = 0$)
$\sigma_{G_W}^2$	Truncated-normal($\sigma_{G_W}^2, \frac{\sigma_{G_W}^2}{20^2}, lower = 0$)
σ_W^2	Truncated-normal($\sigma_W^2, 0.001^2, lower = 0$)
$X_{C(1981)}^1$	Truncated-normal($X_{C(1981)}^1, 2^2, lower = 0$)
$X_{C(1981)}^2$	Truncated-normal($X_{C(1981)}^2, 2^2, lower = 0$)
$X_{C(1981)}^3$	Truncated-normal($X_{C(1981)}^3, 2^2, lower = 0$)
r_S	Truncated-normal($r_S, 0.05^2, lower = 0$)
σ_S^2	Truncated-normal($\sigma_S^2, 0.05^2, lower = 0$)
μ_{G_S}	$N(\mu_{G_S}, 0.05^2)$
ρ_{G_S}	Truncated-normal($\rho_{G_S}, 0.25^2, lower = -1, upper = 1$)
$\sigma_{G_S}^2$	Truncated-normal($\sigma_{G_S}^2, \frac{\sigma_{G_S}^2}{20^2}, lower = 0$)
h_S	Truncated-normal($h_S, 0.25^2, lower = 0$)

Table 9: Proposal distributions of one-pool models used in the CPM method for the Brigalow dataset.

Parameter	Proposal
K_C	$N(K_C, 0.01^2)$
c	Truncated-normal($c, 0.005^2, lower = 0, upper = 1$)
r_W	Truncated-normal($r_W, 0.05^2, lower = 0$)
p	Truncated-normal($p, 0.005^2, lower = 0, upper = 1$)
h_W	Truncated-normal($h_W, 0.1^2, lower = 0$)
μ_{G_W}	$N(\mu_{G_W}, 0.05^2)$
ρ_{G_W}	Truncated-normal($\rho_{G_W}, 0.05^2, lower = -1, upper = 1$)
σ_η^2	Truncated-normal($\sigma_\eta^2, 0.001^2, lower = 0$)
$\sigma_{G_W}^2$	Truncated-normal($\sigma_{G_W}^2, \frac{\sigma_{G_W}^2}{20^2}, lower = 0$)
σ_W^2	Truncated-normal($\sigma_W^2, 0.01^2, lower = 0$)
$X_{C(1981)}^1$	Truncated-normal($X_{C(1981)}^1, 2^2, lower = 0$)
$X_{C(1981)}^2$	Truncated-normal($X_{C(1981)}^2, 2^2, lower = 0$)
$X_{C(1981)}^3$	Truncated-normal($X_{C(1981)}^3, 2^2, lower = 0$)
X_{IOM}	Truncated-normal($X_{IOM}, 0.05^2, lower = 0$)
r_S	Truncated-normal($r_S, 0.05^2, lower = 0$)
σ_S^2	Truncated-normal($\sigma_S^2, 0.01^2, lower = 0$)
μ_{G_S}	$N(\mu_{G_S}, 0.05^2)$
ρ_{G_S}	Truncated-normal($\rho_{G_S}, 0.25^2, lower = -1, upper = 1$)
$\sigma_{G_S}^2$	Truncated-normal($\sigma_{G_S}^2, \frac{\sigma_{G_S}^2}{20^2}, lower = 0$)
h_S	Truncated-normal($h_S, 0.25^2, lower = 0$)

Table 10: Proposal distributions of two-pool models used in the CPM method for the Brigalow dataset.

Parameter	Proposal
$\sigma_{\eta_C}^2$	Truncated-normal($\sigma_{\eta_C}^2, 0.001^2, lower = 0$)
σ_B^2	Truncated-normal($\sigma_B^2, 0.1^2, lower = 0$)
K_B	Truncated-normal($K_B, 0.09^2, lower = 0$)
π_{DB}	Truncated-normal($\pi_{DB}, 0.1^2, lower = 0$)
π_{BB}	Truncated-normal($\pi_{BB}, 0.1^2, lower = 0$)
π_{BC}	Truncated-normal($\pi_{BC}, 0.1^2, lower = 0$)
π_{CB}	Truncated-normal($\pi_{CB}, 0.05^2, lower = 0$)
K_R	Truncated-normal($K_R, 0.1^2, lower = 0$)

Table 11: Proposal distributions of three-pool models used in the CPM method for the Brigalow dataset.

Parameter	Proposal
$\sigma_{\eta_D}^2$	Truncated-normal($\sigma_{\eta_D}^2, 0.02^2, lower = 0$)
$\sigma_{\eta_B}^2$	Truncated-normal($\sigma_{\eta_B}^2, 0.1^2, lower = 0$)
$\sigma_{\eta_R}^2$	Truncated-normal($\sigma_{\eta_R}^2, 0.9^2, lower = 0$)
$\sigma_{\eta_H}^2$	Truncated-normal($\sigma_{\eta_H}^2, 0.1^2, lower = 0$)
$\sigma_{G_W}^2$	Truncated-normal($\sigma_{G_W}^2, \frac{\sigma_{G_W}^2}{30^2}, lower = 0$)
$\sigma_{G_S}^2$	Truncated-normal($\sigma_{G_S}^2, \frac{\sigma_{G_W}^2}{10^2}, lower = 0$)
σ_S^2	Truncated-normal($\sigma_S^2, 0.05^2, lower = 0$)
X_{IOM}	Truncated-normal($X_{IOM}, 0.9^2, lower = 0$)
$X_{C(1981)}^1$	Truncated-normal($X_{C(1981)}^1, 3^2, lower = 0$)
$X_{C(1981)}^2$	Truncated-normal($X_{C(1981)}^2, 3^2, lower = 0$)
$X_{C(1981)}^3$	Truncated-normal($X_{C(1981)}^3, 3^2, lower = 0$)
K_D	Truncated-normal($K_D, 0.005^2, lower = 0$)
K_B	Truncated-normal($K_B, 0.1^2, lower = 0$)
K_R	Truncated-normal($K_R, 0.05^2, lower = 0$)
K_H	Truncated-normal($K_H, 0.01^2, lower = 0$)
h_W	Truncated-normal($h_W, 0.05^2, lower = 0$)
h_S	Truncated-normal($h_S, 0.5^2, lower = 0$)
P_D	Truncated-normal($P_D, 0.15^2, lower = 0$)
π_{DH}	Truncated-normal($\pi_{DH}, 0.09^2, lower = 0$)
π_{RH}	Truncated-normal($\pi_{RH}, 0.1^2, lower = 0$)
π_{HH}	Truncated-normal($\pi_{HH}, 0.1^2, lower = 0$)
π_{BH}	Truncated-normal($\pi_{BH}, 0.15^2, lower = 0$)
π_{RB}	Truncated-normal($\pi_{RB}, 0.09^2, lower = 0$)
π_{HB}	Truncated-normal($\pi_{HB}, 0.1^2, lower = 0$)
ρ_{G_S}	Truncated-normal($\rho_{G_S}, 0.1^2, lower = -1, upper = 1$)

Table 12: Proposal distributions of five-pool models used in the CPM method for the Brigalow dataset.

$\boldsymbol{\mu}$ and covariance matrix $\boldsymbol{\Sigma}$. In Algorithm 1, $\mathbf{K}_{(t)}$ is the Kalman gain matrix, $\mathbf{P}_{(t)}^{t-1}$ and $X_{(t)}^{t-1}$ are the process noise and the expectations of state variable, respectively given all observations up to and including time $t - 1$.

To apply the KF to the Tarlee model, we use a log transformation, i.e. $X^* = \log(X)$ and $Y^* = \log(Y)$ in order to form a linear-Gaussian state-space model for the state-space model

Algorithm 1 Kalman filter algorithm

- 1: Initialize with initial state $\hat{X}_{(0)} = x_{(0)}$ and $\hat{P}_{(0)} = \mathbf{Q}^*$ at $t = 0$;
 - 2: **for** $t = 1, \dots, T$ **do**
 - 3: $X_{(t)}^{t-1} = \mathbf{A}^* \hat{X}_{(t-1)} + \mathbf{B}^* u_{(t)}$, State estimate extrapolation;
 - 4: $\mathbf{P}_{(t)}^{t-1} = \mathbf{A}^* \hat{\mathbf{P}}_{(t-1)} \mathbf{A}^{*'} + \mathbf{Q}^*$, State covariance extrapolation;
 - 5: $\mathbf{K}_{(t)} = \mathbf{P}_{(t)}^{t-1} \mathbf{C}^{*'} [\mathbf{R}^* + \mathbf{C}^* \mathbf{P}_{(t)}^{t-1} \mathbf{C}^{*'}]^{-1}$, Kalman gain matrix;
 - 6: $\hat{X}_{(t)} = X_{(t)}^{t-1} + \mathbf{K}_{(t)} [Y_{(t)} - \mathbf{C}^* X_{(t)}^{t-1}]$, State estimate update;
 - 7: $\hat{\mathbf{P}}_{(t)} = [\mathbf{I} - \mathbf{K}_{(t)} \mathbf{C}^*] \mathbf{P}_{(t)}^{t-1}$, State covariance update;
 - 8: Compute the log-likelihood contribution, $l_{(t)}^{\text{KF}}$, at time t through the density $\text{MVN}(Y_{(t)} - \mathbf{C}^* X_{(t)}^{t-1}, \mathbf{R}^* + \mathbf{C}^* \mathbf{P}_{(t)}^{t-1} \mathbf{C}^{*'})$;
 - 9: The complete log-likelihood can be calculated as $L^* = \sum_t l_{(t)}^{\text{KF}}$
-

formed by the sub-model involving $\{X_G^*, X_W^*, X_P^*, Y_G^*, Y_W^*, Y_P^*\}$. Since $X_{W(t)}^*$ depends on $X_{G(t)}^*$ and because of the auto-regressive structure of the state-space model, we rewrite $X_{W(t)}^*$ as follows

$$X_{W(t)}^{*i} \sim N(\log h + \mu_G + \rho_G (X_{G(t-1)}^{*i} - \mu_G), \sigma_W^2 + \sigma_G^2).$$

We can produce estimators of the state variables in the case of linear and non-linear state-space models through particle filters. The algorithm of one of particle filters is introduced in the next section.

D.2 Bootstrap Particle Filter

In the linear and non-linear cases, particle filters can be used to produce estimators of the state variable $X_{(t)}$ and the simplest form of particle filters known as bootstrap particle filter is applied on non-linear part of the model in this study. The algorithm of bootstrap particle filter is provided in Algorithm 2.

D.3 Correlated Pseudo-marginal Method

When the process and observation models depend on a set of unknown static parameters $\boldsymbol{\theta}$, one can treat the parameters as random variables and utilise Bayesian approach to estimate $\boldsymbol{\theta}$. In the case of having an intractable posterior distribution, numerical methods such as Markov chain Monte Carlo (MCMC) methods can be used. In this study, we utilise correlated pseudo-marginal method, one of the MCMC methods, to generate a sequence of correlated random samples from a probability distribution from which direct sampling is difficult. The likelihood estimators $\hat{p}(\mathbf{Y}|\mathbf{X}, \boldsymbol{\theta}^*)$ and

Algorithm 2 Bootstrap particle filter algorithm

- 1: **for** $k = 1, \dots, N$ **do**
 - 2: $t = 1$, draw sample $X_{(1)}^k \sim p(X_{(1)})$;
 - 3: **for** $t = 2, \dots, T$ **do**
 - 4: **for** $k = 1, \dots, N$ **do**
 - 5: Draw sample $X_{(t)}^k \sim p(X_{(t)}|X_{(t-1)}^{*k})$;
 - 6: Calculate weights $w_{(t)}^k = p(Y_{(t)}|X_{(t)}^k)$;
 - 7: Estimate the log-likelihood component for the t^{th} observation, $\hat{l}_{(t)} = \log \left(\frac{\sum_j w_{(t)}^j}{N} \right)$;
 - 8: Normalise weights $W_{(t)}^k = \frac{w_{(t)}^k}{\sum_j w_{(t)}^j}$ for $k \in \{1, 2, \dots, N\}$;
 - 9: Resample with replacement N particles $X_{(t)}^k$ based on the normalised importance weights;
 - 10: Estimate the overall log-likelihood $L^* = \sum_t \hat{l}_{(t)}$.
-

$\hat{p}(\mathbf{Y}|\mathbf{X}, \boldsymbol{\theta}_{m-1})$ in the acceptance ratio of the CPM method are correlated through correlating the auxiliary random numbers U , used to obtain these estimators, in order to reduce the variance of the resulting ratio. The CPM algorithm is presented in Algorithm 3. To have a highly correlated likelihood estimators in the CPM algorithm it is required to use a particle filter that processes the random numbers in such a manner that the likelihood estimates are similar as possible when slightly perturbing the random numbers. Algorithm 4 shows the particle filter with a given set of random numbers.

Algorithm 3 Correlated pseudo-marginal algorithm

- 1: Initialise $\boldsymbol{\theta}_0$;
- 2: **for** $m = 1, \dots, M^*$ **do**
- 3: Sample $\boldsymbol{\theta}^* \sim Q(\cdot|\boldsymbol{\theta}_{m-1})$;
- 4: Sample $\xi \sim N(\mathbf{0}, \mathbf{I})$ and set $U^* = \tau U_{m-1} + \sqrt{1 - \tau^2} \xi$;
- 5: Compute the estimator $\hat{p}(\mathbf{Y}|\boldsymbol{\theta}^*, U^*)$ using Algorithm 4
- 6: Compute the acceptance ratio:

$$r = \frac{\hat{p}(\mathbf{Y}|\boldsymbol{\theta}^*, U^*)p(\boldsymbol{\theta}^*)Q(\boldsymbol{\theta}_{m-1}|\boldsymbol{\theta}^*)}{\hat{p}(\mathbf{Y}|\boldsymbol{\theta}_{m-1}, U_{m-1})p(\boldsymbol{\theta}_{m-1})Q(\boldsymbol{\theta}^*|\boldsymbol{\theta}_{m-1})};$$

- 7: Accept $(\boldsymbol{\theta}^*, U^*)$ with probability $\min(r, 1)$ otherwise, output $(\boldsymbol{\theta}_{m-1}, U_{m-1})$
-

The process and observation models of the Tarlee and Brigalow datasets are presented in the next sections.

Algorithm 4 Particle filter with fixed random numbers

- 1: Sample $U_{(j^*)} \sim N(0, 1)$ and $V_{(i^*)} \sim N(0, 1)$ for all $j^* \in \{1, \dots, TN\}$ and $i^* \in \{1, \dots, T\}$;
 - 2: Sample $X_{(1)}^k \sim p(\cdot | U_{1:N}, \boldsymbol{\theta})$ for all $k \in \{1, \dots, N\}$;
 - 3: **for** $t = 1, \dots, T-1$ **do**
 - 4: Sort the collection $\{X_{(t)}^1, \dots, X_{(t)}^N\}$;
 - 5: Compute importance weights $w_{(t)}^k$ and log-likelihoods $\hat{l}_{(t)} = \log \left(\frac{\sum_k w_{(t)}^k}{N} \right)$ for $k \in \{1, \dots, N\}$;
 - 6: Sample $X_{(t)}^k$ based on systematic resampling using random values $V_{1:T}$ and normalised weights $W_{(t)}^k$ for $k \in \{1, \dots, N\}$;
 - 7: Set $X_{(t+1)}^k$ as a sample from $p(\cdot | X_{(t)}^k, U_{Nt+1:N(t+1)}, \boldsymbol{\theta})$ for $k \in \{1, \dots, N\}$;
 - 8: Estimate the overall log-likelihood $L^* = \sum_t \hat{l}_{(t)}$.
-

E One-pool Model

E.1 Process Model

The process model of the one-pool model at time t in field (or soil type) i is:

$$\log(X_{C(t)}^i) = \log(X_{C(t-1)}^i e^{-K_C \Delta t} + I_{C(t)}^i) + \eta_{(t)}^i, \quad \eta_{(t)}^i \sim N(0, \sigma_\eta^2); \quad (6)$$

$$X_{G_W(t)}^i \sim LN(\mu_{G_W} + \rho_{G_W}(\log(X_{G_W(t-1)}^i) - \mu_{G_W}), \sigma_{G_W}^2); \quad (7)$$

$$X_{W(t)}^i \sim LN(\log h_W + \log(x_{G_W(t)}^i), \sigma_W^2); \quad (8)$$

$$X_{P(t)}^i \sim LN(\mu_P + \rho_P(\log(X_{P(t-1)}^i) - \mu_P), \sigma_P^2); \quad (9)$$

$$X_{G_S(t)}^i \sim LN(\mu_{G_S} + \rho_{G_S}(\log(X_{G_S(t-1)}^i) - \mu_{G_S}), \sigma_{G_S}^2); \quad \text{and} \quad (10)$$

$$X_{S(t)}^i \sim LN(\log h_S + \log(x_{G_S(t)}^i), \sigma_S^2); \quad (11)$$

where h_W , h_S , ρ_P , ρ_{G_W} , and ρ_{G_S} denote the harvest index which is the ratio of wheat to grain, the harvest index which is the ratio of sorghum to grain, auto-regressive parameters for the evolution of pasture total dry matter (TDM) and grain TDM of wheat and sorghum, respectively. Notice that $X_{W(t)}^i$ and $X_{S(t)}^i$ are defined conditional on $X_{G_W(t)}^i = x_{G_W(t)}^i$ and $X_{G_S(t)}^i = x_{G_S(t)}^i$, respectively. The process of total wheat and sorghum dry matters and the total grain dry matters are separated because of measuring grain yield in spite of that the total wheat and sorghum dry matter contain the total grain dry matters (i.e. $X_{G_W(t)}^i \leq X_{W(t)}^i$ and $X_{G_S(t)}^i \leq X_{S(t)}^i$). Notice that since there is no sorghum crop in the Tarlee dataset, we do not consider process and measurement models of the sorghum in its model. In addition, as there is no pasture in the Brigalow dataset, we do

not consider process and measurement models of the pasture in the model. Therefore, the mass of carbon inputs, $I_{C(t)}^i$, of the Tarlee and Brigalow datasets which are denoted by $IT_{C(t)}^i$ and $IB_{C(t)}^i$ respectively are:

$$IT_{C(t)}^i = \begin{cases} c(X_{W(t)}^i - X_{G_W(t)}^i) + cr_W X_{W(t)}^i & \text{Wheat for Grain} \\ cpX_{W(t)}^i + cr_W X_{W(t)}^i & \text{Wheat for Hay} \\ cX_{P(t)}^i + cr_P X_{P(t)}^i & \text{Pasture} \\ cpX_{P(t)}^i + cr_P X_{P(t)}^i & \text{Pasture for Hay} \\ 0 & \text{Fallow} \end{cases}$$

and

$$IB_{C(t)}^i = \begin{cases} c(X_{W(t)}^i - X_{G_W(t)}^i) + cr_W X_{W(t)}^i & \text{Wheat for Grain} \\ cpX_{W(t)}^i + cr_W X_{W(t)}^i & \text{Wheat for Hay} \\ c(X_{S(t)}^i - X_{G_S(t)}^i) + cr_S X_{S(t)}^i & \text{Sorghum for Grain} \\ cpX_{S(t)}^i + cr_S X_{S(t)}^i & \text{Sorghum for Hay} \\ 0 & \text{Fallow} \end{cases}$$

where p , r_W , r_S , and r_P are the proportion of the crop left above-ground after harvest, the root-to-shoot ratios (in terms of TDM) for wheat, sorghum and pasture crops, respectively. The amount of carbon that enters into the soil from plant-matter that is already below-ground (i.e., roots) and from plant-matter that remains above-ground after harvesting, $c(X_{W(t)}^i - X_{G_W(t)}^i)$ and $c(X_{S(t)}^i - X_{G_S(t)}^i)$, are included in $IT_{C(t)}^i$ and $IB_{C(t)}^i$, respectively. Here c , $(X_{S(t)}^i - X_{G_S(t)}^i)$ and $(X_{W(t)}^i - X_{G_W(t)}^i)$ are the carbon content of dry plant matter and the above-ground plant-matter biomass of sorghum and wheat, respectively.

In this model, $X_{(t)}^i = (X_{C(t)}^i, X_{G_W(t)}^i, X_{W(t)}^i, X_{P(t)}^i, X_{G_S(t)}^i, X_{S(t)}^i)$ is all processes at time t in field (soil type) i . Given a vector of parameters θ for the model, the transition density of the joint process model (which is a discrete-time Markov chain) of the independent processes (6)-(11) can

be written as:

$$\begin{aligned}
p(X_{(t)}^i | X_{(t-1)}^i, \boldsymbol{\theta}) &= p(X_{C(t)}^i | I_{C(t)}^i, X_{C(t-1)}^i, \boldsymbol{\theta}) \times p(X_{G_W(t)}^i | X_{G_W(t-1)}^i, \boldsymbol{\theta}) \\
&\times p(X_{W(t)}^i | X_{G_W(t)}^i, \boldsymbol{\theta}) \times p(X_{P(t)}^i | X_{P(t-1)}^i, \boldsymbol{\theta}) \times p(X_{G_S(t)}^i | X_{G_S(t-1)}^i, \boldsymbol{\theta}) \\
&\times p(X_{S(t)}^i | X_{G_S(t)}^i, \boldsymbol{\theta}).
\end{aligned}$$

The overall transition density is

$$p(X_{(t)} | X_{(t-1)}, \boldsymbol{\theta}) = \prod_{i=1}^3 p(X_{(t)}^i | X_{(t-1)}^i, \boldsymbol{\theta});$$

as the three fields (soil types) are independent. For the sake of simplicity, we use the same notation for the overall transition density in all models.

E.2 Observation Model

The observation model of the one-pool includes the sub-models (12)-(17) to account for measurement error.

$$Y_{TOC(t)}^i | X_{C(t)}^i = x_{C(t)}^i \sim LN(\log(x_{C(t)}^i), \sigma_{\epsilon_{TOC}}^2); \quad (12)$$

$$Y_{G_W(t)}^i | X_{G_W(t)}^i = x_{G_W(t)}^i \sim LN(\log(x_{G_W(t)}^i), \sigma_{\epsilon_{G_W}}^2); \quad (13)$$

$$Y_{W(t)}^i | X_{W(t)}^i = x_{W(t)}^i \sim LN(\log(x_{W(t)}^i), \sigma_{\epsilon_W}^2); \quad (14)$$

$$Y_{P(t)}^i | X_{P(t)}^i = x_{P(t)}^i \sim LN(\log(x_{P(t)}^i), \sigma_{\epsilon_P}^2); \quad (15)$$

$$Y_{G_S(t)}^i | X_{G_S(t)}^i = x_{G_S(t)}^i \sim LN(\log(x_{G_S(t)}^i), \sigma_{\epsilon_{G_S}}^2); \quad \text{and} \quad (16)$$

$$Y_{S(t)}^i | X_{S(t)}^i = x_{S(t)}^i \sim LN(\log(x_{S(t)}^i), \sigma_{\epsilon_S}^2). \quad (17)$$

As the measurements (12)-(17) are independent, the joint observation model of them at time t and field (or soil type) i , conditioning on unobserved variable vector $X_{(t)}^i$ and parameter $\boldsymbol{\theta}$ is:

$$\begin{aligned}
p(Y_{(t)}^i | X_{(t)}^i, \boldsymbol{\theta}) &= p(Y_{TOC(t)}^i | X_{C(t)}^i, \boldsymbol{\theta}) \times p(Y_{G_W(t)}^i | X_{G_W(t)}^i, \boldsymbol{\theta}) \\
&\times p(Y_{W(t)}^i | X_{W(t)}^i, \boldsymbol{\theta}) \times p(Y_{P(t)}^i | X_{P(t)}^i, \boldsymbol{\theta}) \\
&\times p(Y_{G_S(t)}^i | X_{G_S(t)}^i, \boldsymbol{\theta}) \times p(Y_{S(t)}^i | X_{S(t)}^i, \boldsymbol{\theta}); \quad (18)
\end{aligned}$$

where $Y_{(t)}^i = (Y_{TOC(t)}^i, Y_{G_W(t)}^i, Y_{W(t)}^i, Y_{P(t)}^i, Y_{G_S(t)}^i, Y_{S(t)}^i)$. The overall observation model across all i 's is therefore:

$$p(Y_{(t)}|X_{(t)}, \boldsymbol{\theta}) = \prod_{i=1}^3 p(Y_{(t)}^i|X_{(t)}^i, \boldsymbol{\theta}).$$

For notational convenience, we use the same notation $Y_{(t)}$ and $X_{(t)}$ in other models presented below.

F Two-pool Model

F.1 Process Model

The process model of the two-pool model includes the following sub-models

$$\begin{aligned} \log(X_{C(t)}^i) &= \log(X_{C(t-1)}^i e^{-K_C \Delta t} + I_{C(t)}^i) + \eta_{(t)}^i, \quad \eta_{(t)}^i \sim N(0, \sigma_\eta^2); \\ X_{G_W(t)}^i &\sim LN(\mu_{G_W} + \rho_{G_W}(\log(X_{G_W(t-1)}^i) - \mu_{G_W}), \sigma_{G_W}^2); \\ X_{W(t)}^i &\sim LN(\log h_W + \log(x_{G_W(t)}^i), \sigma_W^2); \\ X_{P(t)}^i &\sim LN(\mu_P + \rho_P(\log(X_{P(t-1)}^i) - \mu_P), \sigma_P^2); \\ X_{G_S(t)}^i &\sim LN(\mu_{G_S} + \rho_{G_S}(\log(X_{G_S(t-1)}^i) - \mu_{G_S}), \sigma_{G_S}^2); \\ X_{S(t)}^i &\sim LN(\log h_S + \log(x_{G_S(t)}^i), \sigma_S^2); \quad \text{and} \\ X_{IOM(t)}^i &= X_{IOM(t-1)}^i = M; \end{aligned} \tag{19}$$

where M is an unknown constant value.

F.2 Observation Model

The observation model of the two-pool model includes the following sub-models

$$Y_{TOC(t)}^i | X_{C(t)}^i = x_{C(t)}^i, X_{IOM(t)}^i = x_{IOM(t)}^i \sim LN(\log(x_{C(t)}^i + x_{IOM(t)}^i), \sigma_{\epsilon_{TOC}}^2); \quad (20)$$

$$Y_{IOM(t)}^i | X_{IOM(t)}^i = x_{IOM(t)}^i \sim LN(\log(x_{IOM(t)}^i), \sigma_{\epsilon_{IOM}}^2); \quad (21)$$

$$Y_{G_W(t)}^i | X_{G_W(t)}^i = x_{G_W(t)}^i \sim LN(\log(x_{G_W(t)}^i), \sigma_{\epsilon_{G_W}}^2);$$

$$Y_{W(t)}^i | X_{W(t)}^i = x_{W(t)}^i \sim LN(\log(x_{W(t)}^i), \sigma_{\epsilon_W}^2);$$

$$Y_{P(t)}^i | X_{P(t)}^i = x_{P(t)}^i \sim LN(\log(x_{P(t)}^i), \sigma_{\epsilon_P}^2);$$

$$Y_{G_S(t)}^i | X_{G_S(t)}^i = x_{G_S(t)}^i \sim LN(\log(x_{G_S(t)}^i), \sigma_{\epsilon_{G_S}}^2); \quad \text{and}$$

$$Y_{S(t)}^i | X_{S(t)}^i = x_{S(t)}^i \sim LN(\log(x_{S(t)}^i), \sigma_{\epsilon_S}^2).$$

As it is shown in (20), the observational data TOC depends on the state variables $X_{C(t)}^i$ and $X_{IOM(t)}^i$. Since the measurements (20) and (21) are independent, we compute the joint observation model of the components of this model by multiplying the probability density functions of measurement variables $Y_{TOC(t)}^i, Y_{G_W(t)}^i, Y_{W(t)}^i, Y_{P(t)}^i, Y_{G_S(t)}^i, Y_{S(t)}^i$, and $Y_{IOM(t)}^i$ given their corresponding state variables at time t .

G Three-pool Model

G.1 Process Model

The first pool of this model encompasses components DPM, POC, and HUM. To simplify notation, we keep the latent variable of this pool as $X_{C(t)}^i$ at time t in field (soil type) i . The process model of the three-pool model includes the latent variables $X_{B(t)}^i$ and $X_{C(t)}^i$ along with the latent variables of processes (19) and (7)-(11). The processes of $X_{C(t)}^i$ and $X_{B(t)}^i$ are shown as

$$\begin{aligned} \log(X_{C(t)}^i) &= \log(X_{C(t-1)}^i e^{-K_C \Delta t} + I_{C(t)}^i \\ &\quad + X_{B(t-1)}^i (1 - e^{-K_B \Delta t}) \pi_{BC}) + \eta_{C(t)}^i, \quad \eta_{C(t)}^i \sim N(0, \sigma_{\eta_C}^2); \end{aligned} \quad (22)$$

$$\begin{aligned} \log(X_{B(t)}^i) &= \log(X_{B(t-1)}^i e^{-K_B \Delta t} + X_{C(t-1)}^i (1 - e^{-K_C \Delta t}) \pi_{CB} \\ &\quad + X_{B(t-1)}^i (1 - e^{-K_B \Delta t}) \pi_{BB}) + \eta_{B(t)}^i, \quad \eta_{B(t)}^i \sim N(0, \sigma_{\eta_B}^2). \end{aligned} \quad (23)$$

Notice that the mass of BIO should be less than 5 percent of the total mass of carbon (e.g. $X_{BIO} \leq 0.05X_C$). The transition density of the joint process model of the latent variables in the three-pool model is the product of the transition densities of all state variables in the three-pool model.

G.2 Observation Model

The BIO pool is considered as the third pool in the three-pool model and uncertainty around the observations of the total SOC in field (soil type) i at time t is modeled as follows

$$\begin{aligned}
 Y_{TOC(t)}^i | X_{C(t)}^i = x_{C(t)}^i, X_{IOM(t)}^i = x_{IOM(t)}^i \\
 , X_{B(t)}^i = x_{B(t)}^i \sim LN(\log(x_{C(t)}^i + x_{IOM(t)}^i + x_{B(t)}^i), \sigma_{\epsilon_{TOC}}^2). \quad (24)
 \end{aligned}$$

In addition to sub-model (24), the observation model of the three-pool model includes sub-models (13)-(17) and (21). The joint observation model of the three-pool model can be computed by multiplying the probability density functions of equations (13)-(17), (21), and (24). The next section introduces the process and observation models of the five-pool model in which each SOC component is considered as a pool.

H Five-pool Model

H.1 Process Model

The process model of the five-pool model includes sub-models (19), (7)-(11), and the following sub-models

$$\log(X_{D(t)}^i) = \log(X_{D(t-1)}^i e^{-K_D \Delta t} + P_D I_{C(t)}^i) + \eta_{D(t)}^i, \quad \eta_{D(t)}^i \sim N(0, \sigma_{\eta_D}^2); \quad (25)$$

$$\log(X_{R(t)}^i) = \log(X_{R(t-1)}^i e^{-K_R \Delta t} + (1 - P_D) I_{C(t)}^i) + \eta_{R(t)}^i, \quad \eta_{R(t)}^i \sim N(0, \sigma_{\eta_R}^2); \quad (26)$$

$$\begin{aligned} \log(X_{H(t)}^i) = & \log(X_{H(t-1)}^i e^{-K_H \Delta t} + X_{D(t-1)}^i (1 - e^{-K_D \Delta t}) \pi_{DH} \\ & + X_{R(t-1)}^i (1 - e^{-K_R \Delta t}) \pi_{RH} + X_{H(t-1)}^i (1 - e^{-K_H \Delta t}) \pi_{HH} \\ & + X_{B(t-1)}^i (1 - e^{-K_B \Delta t}) \pi_{BH}) + \eta_{H(t)}^i, \quad \eta_{H(t)}^i \sim N(0, \sigma_{\eta_H}^2); \end{aligned} \quad (27)$$

$$\begin{aligned} \log(X_{B(t)}^i) = & \log(X_{B(t-1)}^i e^{-K_B \Delta t} + X_{D(t-1)}^i (1 - e^{-K_D \Delta t}) \pi_{DB} \\ & + X_{R(t-1)}^i (1 - e^{-K_R \Delta t}) \pi_{RB} + X_{H(t-1)}^i (1 - e^{-K_H \Delta t}) \pi_{HB} \\ & + X_{B(t-1)}^i (1 - e^{-K_B \Delta t}) \pi_{BB}) + \eta_{B(t)}^i, \quad \eta_{B(t)}^i \sim N(0, \sigma_{\eta_B}^2). \end{aligned} \quad (28)$$

The transition density of the joint process model of the latent variables in this model can be gained through multiplying the transition densities of the latent variables in this model as they are independent.

H.2 Observation Model

The observation model of the five-pool model captures the uncertainties in the observations of the carbon input, TOC, POC, HUM, and IOM. The observation models of the carbon input and IOM which are presented by equations (13)-(17) and (21) are the same in this model. The measurement processes of the TOC, POC, and HUM given their related state variables (e.g. $X_{D(t)}^i = x_{D(t)}^i$) are

$$\log(Y_{TOC(t)}^i) = \log(x_{D(t)}^i + x_{IOM(t)}^i + x_{B(t)}^i + x_{R(t)}^i + x_{H(t)}^i) + \eta_{\epsilon TOC}, \quad \eta_{\epsilon TOC} \sim N(0, \sigma_{\epsilon TOC}^2); \quad (29)$$

$$\log(Y_{POC(t)}^i) = \log(x_{D(t)}^i + x_{B(t)}^i + x_{R(t)}^i) + \eta_{\epsilon POC}, \quad \eta_{\epsilon POC} \sim N(0, \sigma_{\epsilon POC}^2); \quad (30)$$

$$\log(Y_{H(t)}^i) = \log(x_{H(t)}^i) + \eta_{\epsilon H}, \quad \eta_{\epsilon H} \sim N(0, \sigma_{\epsilon H}^2). \quad (31)$$

Since the measurement variables in (29)-(31) are independent, the product of the probability density functions of equations (13)-(17), (21), and (29)-(31) yields the joint observation model of the five-pool model.

I Gelman and Rubin's convergence diagnostic statistic

Parameter	\hat{R}	Upper C.I. bound on \hat{R}
K_C	1.00	1.00
c	1.00	1.00
r_W	1.00	1.00
r_P	1.00	1.00
p	1.00	1.00
h_W	1.00	1.01
μ_{G_W}	1.03	1.08
μ_P	1.00	1.00
ρ_{G_W}	1.06	1.16
ρ_P	1.00	1.00
$\sigma_{\eta_C}^2$	1.05	1.07
$\sigma_{G_W}^2$	1.01	1.02
σ_W^2	1.07	1.11
σ_P^2	1.01	1.01
Y_{IOM}	1.00	1.00
$\sigma_{\eta_B}^2$	1.02	1.04
K_B	1.00	1.00
π_{CB}	1.00	1.01
π_{BB}	1.00	1.00
π_{BC}	1.00	1.00

Table 13: The Gelman and Rubin's convergence diagnostic, \hat{R} calculated for model parameters of the three-pool model of the Tarlee dataset. Since the point estimate of \hat{R} for each parameter is less than 1.2, the MCMC samples can be considered to have reached a stationary distribution and are mixing adequately.

J Estimated LPD and ELPD of the models

The mean and standard deviation of the fourchains of the estimated LPD at each time point and the ELPD of the models applied on the Tarleeand Brigalow datasets are shown in Tables 15 and 16, respectively.

Parameter	\hat{R}	Upper C.I. bound on \hat{R}
K_C	1.00	1.00
c	1.00	1.00
r_W	1.00	1.00
p	1.01	1.03
h_W	1.01	1.02
μ_{G_W}	1.10	1.23
μ_{G_S}	1.00	1.00
ρ_{G_W}	1.01	1.03
σ_η^2	1.07	1.19
$\sigma_{G_W}^2$	1.00	1.00
σ_W^2	1.01	1.01
r_S	1.00	1.00
σ_B^2	1.14	1.35
σ_S^2	1.10	1.30
K_B	1.00	1.02
K_R	1.02	1.07
π_{DB}	1.00	1.00
π_{BB}	1.00	1.00
π_{BC}	1.00	1.02
π_{CB}	1.05	1.17
μ_{G_S}	1.00	1.00
ρ_{G_S}	1.00	1.00
$\sigma_{G_S}^2$	1.05	1.07
h_S	1.01	1.02
ρ_{G_S}	1.00	1.00

Table 14: The Gelman and Rubin’s convergence diagnostic, \hat{R} calculated for model parameters of the three-pool model of the Brigalow dataset. Since the point estimate of \hat{R} for each parameter is less than 1.2, the MCMC samples can be considered to have reached a stationary distribution and are mixing adequately.

Time	One-pool model		Two-pool model		Three-pool model		Five-pool model	
	Mean (LPD)	SD (LPD)	Mean (LPD)	SD (LPD)	Mean (LPD)	SD (LPD)	Mean (LPD)	SD (LPD)
13	-5.27	0.44	-3.21	0.27	-2.40	0.04	-2.67	0.02
14	-8.14	0.41	-8.34	0.48	-7.22	0.17	-6.35	0.10
15	-5.53	0.30	-3.72	0.08	-3.26	0.04	-2.85	0.01
16	-7.82	0.41	-7.32	0.77	-6.09	0.24	-6.09	0.27
17	-6.45	0.86	-5.15	0.65	-5.34	0.36	-3.62	0.02
18	-7.70	0.50	-6.42	0.21	-5.11	0.21	-4.97	0.12
19	-5.66	0.44	-3.02	0.11	-2.59	0.03	-3.04	0.03
20	-6.45	0.44	-3.33	0.25	-2.78	0.71	-7.41	0.61
ELPD	-53.02	3.80	-40.55	2.82	-34.79	1.80	-37	1.18

Table 15: The mean and standard deviation (SD) of the four chains of the estimated LPD and ELPD of the SOC models applied on the Tarlee dataset.

Time	One-pool model		Two-pool model		Three-pool model		Five-pool model	
	Mean (LPD)	SD (LPD)	Mean (LPD)	SD (LPD)	Mean (LPD)	SD (LPD)	Mean (LPD)	SD (LPD)
14	-9.82	0.82	-9.93	1.70	-8.62	0.45	-9.60	1.71
15	-7.13	0.22	-6.88	0.14	-6.97	0.34	-7.40	0.43
16	-7.86	0.50	-7.96	0.87	-8.51	0.47	-8.62	0.54
17	-3.69	0.06	-3.71	0.05	-3.77	0.06	-3.94	0.03
18	-6.84	0.28	-6.74	0.05	-6.57	0.56	-7.95	0.98
19	-1.55	0.03	-1.66	0.03	-2.04	0.06	-12.06	0.89
ELPD	-36.89	1.91	-36.88	2.84	-36.48	1.94	-49.57	4.58

Table 16: The mean and standard deviation (SD) of the four chains of the estimated LPD and ELPD of the SOC models applied on the Brigalow dataset.

K Data Availability

Dataset can be accessed online at:

<https://doi.org/10.4225/08/54F0786D6D923>.